UNIVERSIDADE DE SÃO PAULO
INSTITUTO DE FÍSICA DE SÃO CARLOS

BRUNO ANDRADE ONO

Cellulose and chitosan chloride hydrogels applied in tissue engineering

São Carlos
2022

BRUNO ANDRADE ONO

Cellulose and chitosan chloride hydrogels applied in tissue engineering

Thesis presented to the Graduate Program in Physics at the Instituto de Física de São Carlos, Universidade de São Paulo to obtain the degree of Doctor of Science.

Concentration area: Applied Physics
Option: Biomolecular Physics
Advisor:
Prof. Dr. Francisco Eduardo Gontijo Guimarães

Original version

São Carlos
2022

Ono, Bruno Andrade
Cellulose and chitosan chloride hydrogels applied in tissue engineering / Bruno Andrade Ono; advisor Francisco Eduardo Gontijo Guimarães -- São Carlos 2022.
80 p.

Thesis (Doctorate - Graduate Program in Biomolecular Physics) -- Instituto de Física de São Carlos, Universidade de São Paulo - Brasil , 2022.

1. Chitosan chloride. 2. Cellulose. 3. Hydrogels. 4. Tissue engineering. I. Guimarães, Francisco Eduardo Gontijo , advisor. II. Title.

FOLHA DE APROVAÇÃO

Bruno Andrade Ono

Tese apresentada ao Instituto de Física de São Carlos da Universidade de São Paulo para obtenção do título de Doutor em Ciências. Área de Concentração: Física Aplicada - Opção: Física Biomolecular.

Aprovado(a) em: 27/05/2022

Comissão Julgadora

Dr(a). Francisco Eduardo Gontijo Guimarães

Instituição: (IFSC/USP)

Dr(a). Ram Sharma

Instituição: (Minaris Regenerative Medicine/Estados Unidos)

Dr(a). Antonio Riul Junior

Instituição: (UNICAMP/Campinas)

Dr(a). Sergio Paulo Campana Filho

Instituição: (IQSC/USP)

Dr(a). Sebastião Pratavieira

Instituição: (IFSC/USP)

ACKNOWLEDGEMENTS

I here deeply express my gratitude to my family, in special, to my parents, Sonia and Armando, who were always cheering for my success. To my brothers who supported me during this stage of my life, even most of the time apart, they loved and cared for me. I feel lucky to have my brother Roberto and Carlos as my biggest friends since I was born. They always give me good advices.

A special thanks to Dr. Danilo Martins dos Santos, Dr. Andrea de Lacerda, Dr. James C. Courtenay, and Dr. Marcus John, who helped me during different stages of this research. I am also thankful to the professors Dr. Sergio Paulo Campana-Filho, Dr. Janet L Scott, Dr. Ram Sharma and my advisor Dr. Francisco Eduardo Gontijo Guimarães. They guide me each one with their best knowledge of the subject and this thesis is the result of profound collaboration.

I am very grateful to have known Prof. Dr. Janet L. Scott. She was an inspiration as scientist and person. I will not forget the morning's meetings at her office and how I felt motivated to do better and more every time I left her office. My time in Bath was great, because of her.

This study was only possible because of the highly skilled people and good infrastructure of the University of Bath, The Brazilian Nanotechnology National Laboratory, the São Carlos Institute of Chemistry and the São Carlos Institute of Physics where this research was made.

I am also thankful to my friends Hashi, Naiara, Italo, Tom, Rafael, Felipe and Mari, who I passed most of my days with and shared the best memories. I will never forget the time I had with Naiara and Italo at our house in São Carlos, taking care of plants, preparing meals and sharing stories.

This study was financed in part by the Coordenação de Aperfeiçoamento de Pessoal de Nível Superior – Brasil (CAPES) - Finance Code 001 and the Bath International Research Funding Schemes supported by Santander.

“If we knew what it was we were doing,
it would not be called research,
would it?”
Albert Einstein (1879 - 1955)

ABSTRACT

ONO, B. A. **Cellulose and Chitosan Chloride Hydrogels Applied in Tissue Engineering.** 2022. 80 p. Thesis (Doctor in Science) - Instituto de Física de São Carlos, Universidade de São Paulo, São Carlos, 2021.

The present study researches a low-cost membrane of cellulose and chloride chitosan for cell growth. This material was used as cell's support without growth factors and using only the physical and molecular properties interactions to promote cell's adhesion and development. The quaternized chitosan derivative was synthetized with two different molecular properties: linear density of positive charge and molecular weight. The interaction of cellulose and these synthetized chitosan lead to four different hydrogels through the combination of these properties. Firstly, the molecules of chitosan were synthetized and characterized by different biophysics techniques as RMN and FT-IR. Secondly, the material was also characterized to understand the interaction between cellulose and chitosan derivates molecules to develop the membrane with the help of confocal microscopy. Lastly, the interaction of these membranes with human cells (MG63) and bacteria (E. coli) was tested to observe the biological response to this new support. The results of synthesis indicate a chitosan derivative with 8% to 40% of positive linear density and a molecular weight around 400 and 900 kg/mol. The higher cell attachment (near to 60%), low cytotoxicity and high cell spreading was observed for the higher DQ similar to the tissue culture plate. The gram-negative bacteria (E. coli) had the biggest damage at higher DQ membranes, however the same material presented the higher number of E. coli attach to it. These results present a low-cost natural source of biomolecules which have nowadays high technologic impact and could be used for developing a potential membrane for tissue engineering. This study was only possible through national and international collaboration with researchers from the University of Bath and the São Carlos Institute of Chemistry.

Keywords: Chitosan chloride. Cellulose. Hydrogels. Tissue engineering.

RESUMO

ONO, B. A. **Hidrogéis de celulose e derivados de quitosana aplicados na engenharia de tecidos.** 2022. 80 p. Tese (Doutorado em Ciências) - Instituto de Física de São Carlos, Universidade de São Paulo, São Carlos, 2021.

O presente estudo pesquisa uma membrana de baixo custo de celulose e cloreto de quitosana para o crescimento celular. Este material foi utilizado como suporte celular e sem fatores de crescimento, utilizando apenas as interações físicas e moleculares para promover a adesão e o desenvolvimento celular. Os derivados quaternizados de quitosana foram sintetizados com duas propriedades moleculares diferentes: densidade linear de carga positiva e peso molecular. A interação da celulose com a quitosana sintetizada leva a quatro hidrogéis diferentes através da combinação dessas propriedades. Primeiramente, as moléculas de quitosana foram sintetizadas e caracterizadas por diferentes técnicas biofísicas como RMN e FT-IR. Em seguida também foi caracterizada, com o auxílio da microscopia confocal, a interação entre as moléculas de celulose e derivados de quitosana para desenvolvimento da membrana. Por fim, a interação dessas membranas com células humanas (MG63) e bactérias (E. coli) foi testada para observar a resposta biológica a este novo suporte. Os resultados da síntese indicam um derivado de quitosana com 8% a 40% de densidade linear positiva e peso molecular em torno de 400 e 900 kg/mol. A maior adesão celular (próximo a 60%), baixa citotoxicidade e alta disseminação celular foi observada para o maior DQ semelhante à placa de cultura de tecidos. As bactérias gram-negativas (E. coli) foram as mais danificadas no material com maior DQ fundido, porém o mesmo material apresentou o maior número de E. coli aderidas a ele. Esses resultados apresentam uma fonte natural de biomoléculas de baixo custo que hoje tem alto impacto tecnológico e podem ser utilizadas para o desenvolvimento de uma membrana potencial para engenharia de tecidos. Este estudo só foi possível através da colaboração nacional e internacional com pesquisadores da Universidade de Bath e do Instituto de Química de São Carlos.

Palavras-chave: Quitosana. Celulose. Hidrogéis. Engenharia de tecidos.

LIST OF FIGURES

LIST OF TABLES

LIST OF ABBREVIATIONS AND ACRONYMS

2P	2 photons
AFM	Atomic force microscopy
Ch	Chitosan
CLSM	Confocal laser scanning microscopy
DD	Deacetylation degree
DQ	Degree of quaternization
D_2O	Deuterium oxide
DMSO	Dimethyl sulfoxide
[EMlm][OAc]	1-ethyl-3-methylimidazolium acetate
FBS	Fetal bovine serum
FLIM	Fluorescence-lifetime imaging microscopy
FT-IR	Fourier-transform infrared spectroscopy
GlcN	D-glucosamine
GlcNAc	N-acetyl-D-glucosamine
Hac	Acetic acid
QCh	N-(2-hydroxy)-propyl-3-trimethylammonium chitosan chloride
MTT	3-(4,5-dimethylthiazol-2-yl)-2,5-diphenyltetrazolium bromide
MW	Molecular weight
NMR	Nuclear magnetic resonance
RMS	Root mean square
TCP	Tissue Culture Plate
UV-VIS	Ultraviolet-visible

CONTENTS

1 INTRODUCTION

Organs transplant is a world-wide problem due to the lower number of organs donated every year do not supply all demand. Then allograft and xenograft materials are frequently used. However, the use of these materials do not possess a long durability, because the cells do not survive too long inside the materials and could be rejected by the immune system of the patient. (1) This worldwide problem affects people, who normally wait for skin, heart, kidneys and other important organs to live. Adding the downside of regularly treatments such as hemodialysis for the patient to stay health and leading pressure and cost aggregate for health public system.

The recent advances in tissue engineering are blooming in the regenerative field. The organs development and synthetic tissue generated with cells from the own donors is a challenge for different research groups around the world. (2-5) The studies are researching methods for growing the patient cells inside the laboratory and insert into 2D and 3D platforms leading to the development of tissues and organs. However, the interaction among cells, other tissues and extracellular matrix is a challenge. (6)

These advances in technology are bringing possibilities to print out functional 3D organs, but they still present some limitations directly linked to the complexity of the organ. Hard tissues as bones presented so far, the best results to recreate structures for transplantation. (7) However, this field still has challenges to recreate complex tissues as muscle, skin and kidney because of the architectural arrangement of cells layers and their connections.

Fundamental research is still being made to choose the materials which have the best properties to provide biocompatibility, since they must allow cells to adhere, divide and spread across it. Many researchers already could turn materials biocompatible through the linking proteins approach (8), which is similar to Tissue Culture Plates (TCP) plates, where a thin layer of proteins from culture media serum coat the plate's surface and the cells attach to it. (9) However, this could increase costs and the temperature variation could damage the proteins.

Here we present a ligand-free material for tissue engineering. These materials are bringing important approaches for the development of tissue-like materials,

numerous studies are being researching the surface interactions between cells and synthetic materials to provide important parameters to generate these materials. (10) Nowadays, cell-responsive hydrogels are emerging for this use with the use of cellulose and chitosan, since these biopolymers could mimic an extracellular matrix (ECM) environment. (11)

The biopolymers used in this study are cellulose and chitosan, both are polysaccharides. Cellulose (Figure 1) is a linear polymer composed of linked β-(1→4) D-glucose units, this molecule has an important structural function in nature as cell wall and it is synthetized by plants, bacteria, algae and oomycetes. Used on large scale by companies, this biomolecule is present in inks, thickening agents, paper, clothes and many other applications.

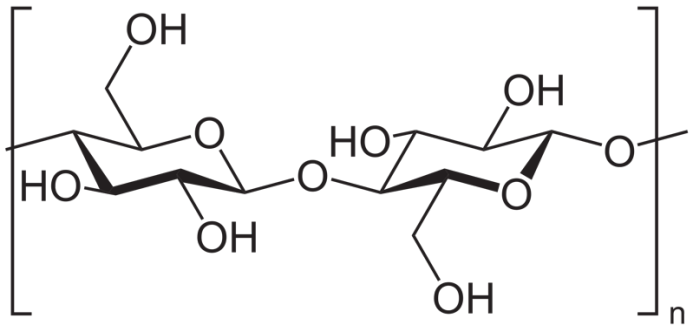

Figure 1 - Cellulose structure formula

Source: NEUROTIKER (12)

Chitosan (Figure 2) is a linear polymer composed of D-glucosamine (GlcN) and N-acetyl-D-glucosamine (GlcNAc) units linked by β-(1→4) linkage. This molecule is frequently obtained by hydrolysis reactions in an alkaline medium, which occurs deacetylation of acetamide groups. However, the number of these two units depends on the reaction condition and rarely is obtained a chitosan totally deacetylated, because of this the molecule properties change.

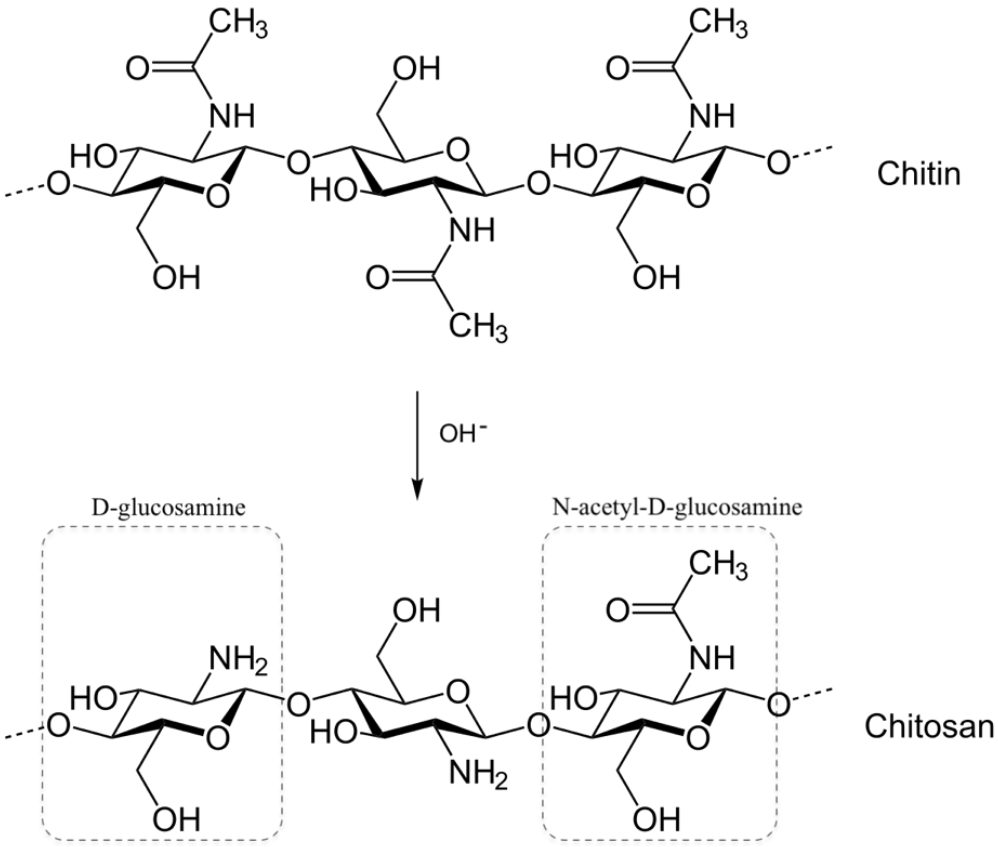

Figure 2 - Chitin reaction in alkaline medium leading to Chitosan molecule represented as structure formula, a polysaccharide composed of N-acetyl-D-glucosamine and D-glucosamine.

Source: Adapted from NEUROTIKER (13)

Charges on a material surface plays an important role in cell adhesion. Some studies revealed the effect between negative and positive charges on polymers when interacting with mammalian cells. (14-15) When an electric field is applied to a surface with cells, they tend to migrate to the positive side. (16) Also is already known that positive charges could interact with bacterial membranes and damage them leading to an antimicrobial effect. (17) Molecular weight and the amino groups are parameters reported in the literature to differentiate biologic properties of chitosan as antimicrobial effect and biodegradability. (18) Amino groups are commonly as an antimicrobial effect agent, because of their positive charge in acid medium, because of this, the polymer could be enhanced effect by inserting positive charges at the polymer. (19)

Through this study we have synthetized and investigate a new compound derivate from chitosan, the N-(2-hydroxy)-propyl-3-trimethylammonium chitosan chloride (QCh) (Figure 3) obtained through reaction with glycidyltrimethylammonium

chloride (GTMAC), which has positive charges and high molecular weight. It is important to note that achievement of high molecular weights is not easily accessible, since the highest sold nowadays are around 375 kDa. Here we studied chitosan of molecular weight up to 1000 kDa obtained through the collaboration with Physical-Organic Chemistry Group of IQSC-USP. (20)

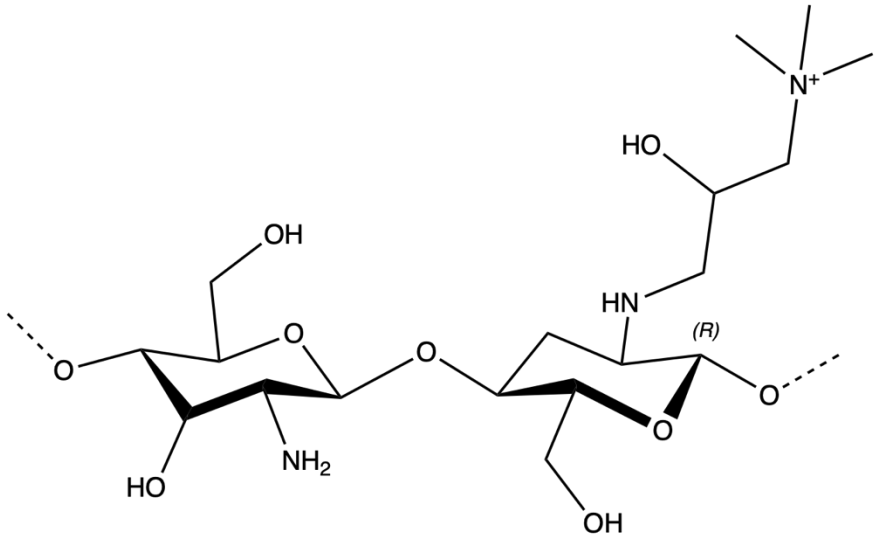

Figure 3 - N-(2-hydroxy)-propyl-3-trimethylammonium chitosan chloride structural formula

Source: By the author

Important parameters to characterize this chitosan molecule are molecular weight, degree of deacetylation (DD) in equation 1 and the degree of quaternization (DQ) in equation 2. The last equation is a specific measure for this new chitosan derivative to measure the linear density of charge.

$$DD(\%) = \left(1 - \frac{I_{CH_3}/3}{I_{H2-H6}/6}\right) X\ 100 \quad (1)$$

$$DQ(\%) = \left(\frac{I_{H1'}}{I_{H1'} - I_{H1}}\right) X\ 100 \quad (2)$$

Cellulose and chitosan are carbohydrates biocompatible with tissues. These polymers have characteristics for cell adhesion, which one of them presents hydrophobicity with tissues. (21-22) There are already at literature studies about the interaction of cellulose among bone, skin and liver cells. (18-19,23) They are already known as biopolymers used for different applications. (26) Here we observe another important use for tissue engineering purpose.

The diversity of applications is related to easy chemical modification of the biopolymer chain. This modification could alter important chemical and physical properties such as charge, molecular size, hydrophobicity and lipophilicity. Our collaborators at the University of Bath developed a biological system, which there is interaction between the modified cellulose by glycidyltrimethylammonium chloride (GTMAC) and mammalian cells. Now they are developing a method to use common printer to create patterns above cellulose sheets using GTMAC (10). The improvement for a better interaction is being studied. (27-32)

Cells scaffolds are highly researched in the tissue engineering field to accommodate and promote cells attachment and growth. These researches revealed the importance of physical properties, such as cyclic strain and stiffness to develop synthetic tissues. (33-34) They also pointed out different types of tissues could respond differently to the same scaffold. (35)

The hydrogels are flexible and constituted by an interconnected structure. They have the advantage of higher water absorption, they do not dissolve in liquids and have resistance to temperature variation, showing a good stability. These properties are similar to natural tissues and due to this, they could be used as bandages. (36) The modification at the molecular level controls properties as mechanical, biodegradation and response to biologic stimulus. Furthermore, the creation of patterns above the hydrogel could mimic the complexity of a tissue and guide tissue growth. (37-38)

Phase-inversion casting is the technique utilized in this study to generate hydrogels membrane (Figure 4), in which there is a transformation of polymer in a liquid phase to a solid phase. The immersion precipitation is one of the four other types of phase-inversion, in which a polymer solution is casted in a support and

submerged in a coagulation bath containing nonsolvent. The exchange between nonsolvent and solvent leads to a precipitation and a membrane is generated.

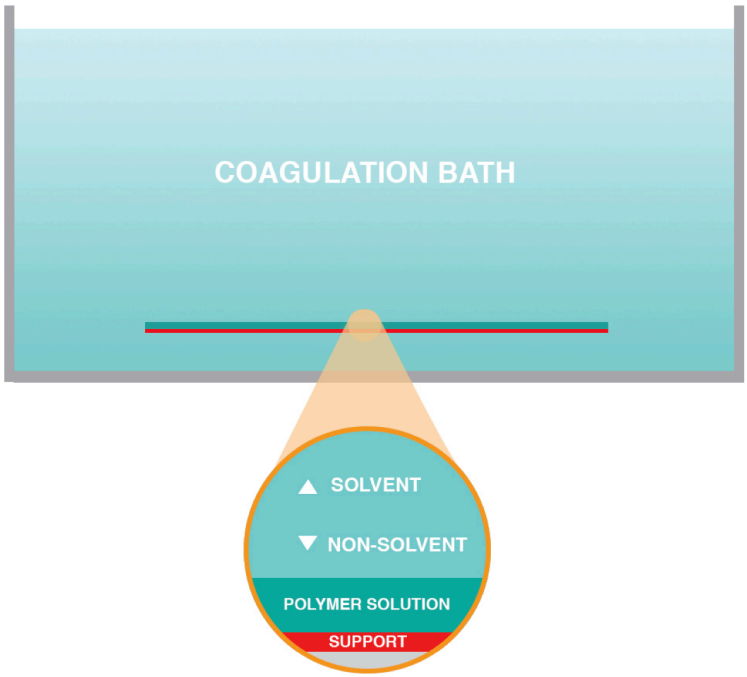

Figure 4 - Phase invert casting technique to produce hydrogels.

Source: By the author.

It is fairly understood that scaffolds are only good, as a biomaterial, if the cells could interact and proliferate with them. From the cells point of view, this biological process is rather complex. The first contact between cells and the material surface is a critical point, because without a proper environment the cells could not adhere and there will not be signaling to proliferate and differentiate.

Those molecular signaling are only reached when proteins called integrins, which are linked indirectly to cytoskeleton, could bind to an extracellular environment. They are transmembrane proteins that are not used only for binding, but have a major response in passing signals to the cell's interior and exterior. The signals could be to tighten or loosen cell grip. However, the principal signaling for tissue engineering it is the activation for proliferation. Without this grip and even supplementing the media with growth factors, the cells will start programmed cell death.

2 RESEARCH OBJECTIVES

The present study is another step in the development of the tissue engineering field using two plentiful and low-cost biomolecules, cellulose and chitosan, to produce a membrane that could support cell's adhesion and growth. This study had different objectives in each step of the research. First, the objective was to synthetize and characterize the properties of chitosan chloride derivative through biophysical analyses. This was made of by getting important parameters such as DQ, molecular weight, fluorescence spectra and others. The second objective was to obtain a stable cellulose membrane casted with these synthetized biopolymers and to observe the interaction between them, as the penetration of chitosan derivative at hydrogel and the mobility of charges at the surface. Next, patterns were printed using these synthetized biopolymers to research new functionalities and uses to these membranes. Finally, the biological effect of these membranes in contact with cells and bacteria was observed to conclude the use for tissue engineering purposes.

3 MATERIALS AND METHODS

3.1 Chitosan Chloride: Synthesis of N-(2-hydroxy)-propyl-3-trimethylammoniumchitosan chloride (QCh)

The synthesis of chitosan derivative with a positive charge is applying another function to this biopolymer, which has numerous applications in technology and could have advantages for tissue engineering. Here, the N-(2-hydroxy)-propyl-3-trimethylammoniumchitosan chloride (QCh) was synthesized by reacting glycidyltrimethylammonium chloride (GTMAC) and chitosan (Ch) in acid medium according as reported by (39), with modifications. 4 g of chitosan was suspended 400 mL of deionized water and 2 mL of glacial acetic acid were added to the suspension, which was kept at constant stirring for 12 h at room temperature. Then, the aqueous solution of GTMAC was added dropwise to the chitosan solution, which was kept under constant stirring at 80 °C for 8 h. Acetone excess was then added to the reaction medium to result in product precipitation, which was filtered, thoroughly washed with acetone and dried in a stove at 35 °C for 24 h. Aiming to produce two QCh samples possessing different average degree of quaternization ($\overline{DQ}$), the synthesis was carried out by using the following reaction conditions: i) sample QCh1: molar ratio GTMAC/chitosan = 3/1; ii) sample QCh2: molar ratio GTMAC/chitosan = 6/1. Then the solutions were dissolved in deionized water until the concentration of 40 mg/mL and degraded in an ultrasound reactor at 200 W of potency and 0.5 of amplitude for 4 h. After this, the powders were obtained by freeze-drying process after passing the solutions through 0.45 μm pore size filters. This was realized in collaboration with Prof. Dr. Sergio Paulo Campana-Filho and Dr. Danilo Martins dos Santos and Andrea de Lacerda at IQSC facilities.

3.2 Molecular weight, deacetylation degree (DD) and degree of quaternization

Molecular weight, deacetylation degree and degree of quaternization are important parameters to compare among different chitosan and studies because they highly influence the phenomena revealed and could help explain the observations. Each powder obtained previously was measured using proton NMR (H-NMR). The

proton measurement was acquired by dissolving the powder in D_2O with 1% (v/v) of HCl at 85 ºC. The spectra were collected with water suppression and Pre-saturation frequency at 4.25 Hz. Using equations 1 and 2 was possible to calculate the degree of quaternization and deacetylation.

The peak of anomeric hydrogen (H1) bonded to unsubstituted glucosamine (GlcN) unit was integrated at ≈ 4.8 ppm, while when substituted in GlcN units was integrated at ≈ 5 ppm. The peak of methyl hydrogens of N-acetyl-D-glucosamine (GlcNAc) units (CH_3) was integrated at ≈ 2 ppm and the peak of hydrogens among other carbons (H3-H6) was integrated at ≈ 3.3 – 4 ppm.

The powder of chitosan and low DQ chitosan were dissolved at 1% (v/v) HAc. The power of high DQ chitosan were dissolved at 1% HCl (v/v). Equation 3 was used to measure the degree of quaternization, in which the methyl groups of substituted GTMAC were integrated at ≈ 55 ppm and the anomeric carbon peak was integrated at ≈ 70 ppm.

$$DQ\ (\%) = \left(\frac{I_{Me_3N_+}/3}{I_{C1}} \right) X\ 100\ (3)$$

Titration experiments were performed by measuring the counter-ions Cl^- ions through a standardized aqueous $AgNO_3$ solution. The powders were dissolved in deionized water and the solution conductivity was measured by adding $AgNO_3$ solution and reading at Handylab LF1 conductivimeter (Schott-Gerate). The degree of quaternization was determined by the following equation:

$$DQ(\%) = \left(\frac{1.7x10^{-5}\ V_{AgNO_3}}{W(g) - (1.7x10^{-5}\ V_{AgNO_3}\ x\ M_{CGTMA})\Big/((M_G x DD) + M_{AG}(1 - DD))\ x\ DD} \right) x100\ \ (4)$$

The molecular weight was determined by measuring intrinsic viscosities [**η**] by

dissolving the polymer in acetic acid and sodium acetate buffer at the proportion of 2:3 [mol.L^{-1}]. The chitosan solution passed by a filtration through 0.45 μm membrane. A glass capillary containing the polymer solution was immersed in a water bath at 25 ºC. The AVS-350 viscometer coupled to the AVS-20 automatic burette (Schott-Gerate, Germany) was used to measure the viscosity by a serial dilution in buffer solutions. The reduced viscosity curve of (η_{sp}/C) against concentration (C) determined the intrinsic viscosities [η]. This was realized in collaboration with Dr. Danilo Martins dos Santos.

3.3 Hydrogel assembly

The phase inverse casting technique was used to generate the hydrogels, a typical method to produce membranes. The ionic liquid of cellulose solutions (4 % wt) were dissolved in DMSO and [EMlm][oAc] electrolytes at the proportion 35:65 (wt %) [EMlm][oAc]/DMSO. The dissolved solution with a transparent and brownish appearance was obtained through shaking and overnight resting. The quaternized chitosan derivative powders with a higher DQ were dissolved easily into PBS and for those with a lower DQ, the addition of 5 % (wt) of HAc was necessary for a better dissolution. Then, the ionic liquid was poured into a rigid glass plate and spread using a doctor blade of 200 μm in height. The plate (Figure 5A) was then submerged in synthetized chitosan solutions of 0.1 % (wt) and a stable film was formed, but physically fragile. The constituted hydrogel was kept in a glass flask with 0.1 % of N_3Na to prevent contamination (Figure 5B).

The interaction between cellulose and chitosan was measured by ninhydrin reaction, in which the amine groups react with ninhydrin and the purple product is obtained. The solution of ninhydrin 2 % (w/v) in methanol was prepared and poured into the hydrogel, then it was incubated for 5 min and dried at 80 ºC. This was realized in collaboration with Dr. Ram Sharma, Dr. Janet Scott and her PhD students Marcus A. John and James C. Courtenay.

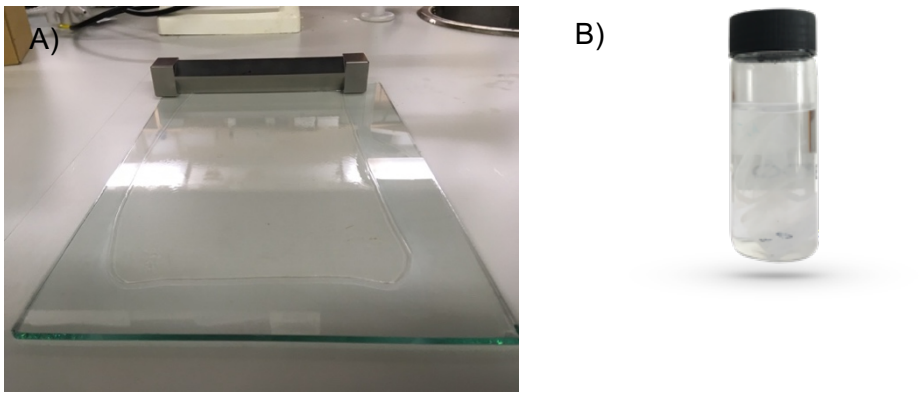

Figure 5 - Hydrogel preparation. a) Ionic liquid spread above a glass plate using a doctorblade and b) constituted hydrogel membrane storaged with sodium azide solution (0.1%).

Source: By the author.

3.4 UV-VIS

The supernatant of storage solution could reveal a possible exit of QCh from the hydrogels. Thus, the spectra were acquired in a spectrophotometer (Varian 50 Bio, Cary) with quartz cuvette and water baseline. The supernatant spectra of storage hydrogel solutions and prepared high DQ QCh solutions 0.1% (wt) were compared.

3.5 Confocal microscopy

Confocal technique is a powerful optical technique, which reveals not only the fluorescence, but also sections from objects observed. Using this experiment we were be able to analyze the hydrogels and cells. The inverted Zeiss LSM 780 confocal laser scanning microscope (CLSM) is equipped with a Coherent Chameleon laser (Ti:sapphire, 80 MHz repetition rate) as a two-photons (2P) excitation source tuned to a wavelength of 800 nm and a diode laser at 405 nm. The images were collected in spectral mode and channel modes with an objective lens (63×, 1.2 numerical aperture, water immersion). The optical setup was adjusted to the best signal-to-noise ratio and fixed when different samples were compared in both CLSM and FLIM modes. A Z-Stack mode was performed to capture confocal planes of the hydrogel with a pace of 5 μm in order to construct a 3D image. The spectral image contains information of fluorescence spectra for each image pixel of the hydrogel confocal plane.

The hydrogels were round shape cut and placed inside a multi-well plate (24), then 8.10^6 cells/ml of E. coli (0.01 Abs) was placed inside the well, which was filled with agar medium. The plate was incubated for 24h at 37 C with low rotation. After the incubation, the medium was removed and the hydrogels were gently washed. The final measurement water volume for each well was 200 µl. Cell viability was measured using the LIVE/DEADTM reagent with 2-photon excitation at 800 nm in channel mode, fluorescence was captured between 415 and 540 nm for acridine orange and 580 to 620 nm for ethidium bromide. The experiments were carried out in the case of viability above 90%.

3.6 AFM Microscopy – Capacitive coupling measurement

This measurement will analyze roughness and charge mobility above the surface of hydrogel and because of it could preview the first interactions between the material's surface and other objects. The hydrogels samples analyzed were the ones casted with 0 % DQ Ch, 9 % DQ QCh and 40 % DQ QCh. First, the hydrogels samples were cut and lyophilized overnight before the imaging process. One area of 5 µm x 5 µm for each hydrogel was measured using a FlexAFM (Nanosurf, Liestal, Switzerland) Atomic Force Microscope (40-41) and PPP-EFM-W probe (Nanosensors, Schaffhausen, Switzerland) with spring constant and resonance frequency of, respectively, 2.8 N/m and 75 kHz. The scans were performed in an environment with a fixed humidity among 60 ± 5 % at 25ºC. Humidity variation was also analyzed by injecting water vapor.

The AC electrical potential with 17 kHz was obtained by deducing the DC signal applied to the cantilever at 17 kHz. The interaction between the sample and the electrified tip was analyzed by the second harmonic of AC signal 34 kHz, which is proportional to the capacitive gradient (dC/dZ).

Kelvin force was measured using the intermittent contact mode setup, slightly below the frequency of resonance. The topography was measured using the intermittent contact mode setup, slightly below the frequency of resonance. The images were analyzed using Gwyddion software. (42) The chamber humidity was changed by injecting water vapor. The materials were evaluated through roughness average (S_a) equation 5 and the root square mean (RMS).

$$S_a = \frac{\sum_{l=0}^{N-1} |z(x_l)|}{N} \quad (5)$$

The roughness average is the sum of all points in a determined area, which is an absolute value and expresses the difference between the heights of each point compared to the arithmetical mean of the surface. This value is a general description of the height variation above the material surface. The measurements were taken at The Brazilian Nanotechnology National Laboratory (LNNano/CNPEM).

3.7 FT-IR characterization

This another technique get a “finger-print” of a molecule and reveals the chemical groups of the samples important to analyze, as the ammonium group inserted at biopolymer chain and other important groups. To obtain this spectrum, the hydrogels membranes were freeze-dried and the powders did not need any preparations. The measurements were taken at ThermoNicolet AVATAR 370 with 50 scans and a resolution of 4 cm^{-2}. The data were fitted through Gaussian curves to measure the different peaks among samples.

3.8 Cell line

The osteosarcoma cell line MG63 (ATCC, USA) and fibroblast cell line HFF-1 (ATCC, USA) were maintained with DMEM supplemented with 10% serum fetal bovine, 1% antibiotics, 1% non-essential amino acids and 1% of sodium pyruvate and incubated at 37 ºC and 5 % CO_2.

3.9 Cell counting

Cells attachment is the first phenomenon important to observe, since it is the first-time cells interact with the material. To perform this experiment, each hydrogel, previously obtained, was cut in 6 round shape pieces and sizes of the multiplates

bottom wells and placed on the bottom of the plate. Then they were incubated overnight on PBS at 37 ºC and 5% of CO_2. After it, they were washed 2 more times with PBS and MG-63 cells were seed at $20x10^3$ cells/cm^2 per one hour above the films with the cell medium.

The medium was gently removed and the cells were fixed (3.7% formalin). The cell nucleus was stained with DAPI (0.2 ng/ml for 5 min) and imaged in a fluorescence microscopy with ex/em 357/447 nm. 5 images were taken for each hydrogel. Then the images were treated with ImageJ software (43), in which they were transformed into 8-bit (Figure 6) color and the threshold was used to differentiate between background and nucleus fluorescence. After this, the counting function was applied for objects with circularity between 0.5 – 1 and sizes above 50 pixels.

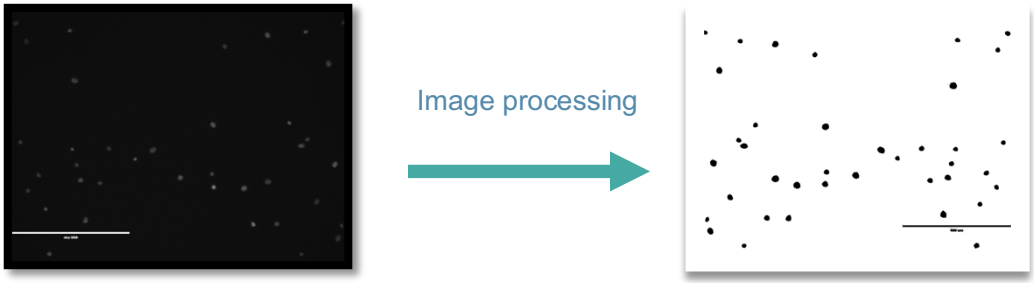

Figure 6 - Imaging process to count the number of cells. Each white spot is the nucleus cell's flourescence

Source: By the author.

3.10 Cell morphology

After cell attachment, we want to observe how they will grow and proliferate above the material, because the cell's shape indicates health and they not start programmed cell death. First, each hydrogel was cut in 6 round shape pieces and sizes of the well of multiplate wells and placed on the bottom of the plate. Then they were incubated overnight on PBS at 37 ºC and 5% of CO_2 and washed 2 more times with PBS before use, after this MG-63 cells were incubated $5x10^3$ cells/cm^2 per one hour above the films with medium, after it the cells were fixed (3.7% formalin) and the nucleus and cytoskeleton were stained, with respectively, DAPI and Phalloidin. Fluorescence microscopy images were acquired with ex/em 357/447 nm for DAPI and ex/em 470/525 nm for Phalloidins FITC.

Cell morphology was acquired through the free software ImageJ. The nucleus

and cytoskeleton images were merged and then transformed to an 8-bit scale. Then the threshold was adjusted to separate the background from the cell's fluorescence by using the ROI manager, the cells were selected using the wand tool from the software.

The circularity (equation 6) was acquired and plotted in a box plot graph. At least 3 images were acquired from each sample. The cell spreading for a cell is measured by circularity, which varies between 0 and 1. The more circularity near to 0, the more spread is the cell and the more near to 1 indicates a round cell shape.

$$Circularity = \frac{4\pi Area}{P^2} \quad (6)$$

3.11 MTT

MTT was performed to measure the cells viability when interacting with hydrogel. The cells were incubated at a cell density of $5x10^3$ cells/cm^2 for 4 days above hydrogels casted with chitosan, low DQ QCh, high QCh and the Tissue Culture Plate (control). Medium was replaced at the second day to secure medium for all cells through the incubation period. After this, the cells were incubated with the MTT solution 0.1mg/ml for 4h and formazan salts were diluted with DMSO. Reads at 570 nm absorbance minus plate absorbance at 670 nm were obtained at a spectrophotometer (Multiskan GO, ThermoScientific). Group viability was determined by the ratio absorbance between the tested group and the control group.

3.12 Pattern above hydrogel

The different connections between tissues is a complexity to develop a synthetic one. Nowadays, recent advances allowed printing different patterns and giving new uses for a membrane. This possibility leads us to experiment how feasible cellulose hydrogels casted with chitosan derivatives could bring new uses. The pattern above the casted membrane was printed using the Autodrop (Microdrop

Technologies, Germany). Tests was performed using water (Figure 7) before to obtain a line pattern. The best configuration to generate the line pattern above the hydrogels was with frequency of 1000 drops/s, 100 drops/position, a negative pressure of -16 mbar to prevent dripping from the tip and a voltage of 83 V to generate round shape drops. Firstly, the solution of 40 % DQ QCh was dissolved in PBS of 0.1 % (wt), filtered in .45 µm filter and inserted in the ink reservoir. Then, the ionic liquid was spread above a glass plate with doctorblade and inserted at Autodrop table to initiate the printing. After lines were printed, the ionic liquid was reconstituted in deionized water, then membranes in round shape was cut and inserted in TCP plates. The lineage of HFF-1 cells was seeded with medium for 24 h, and MTT reagents was incubated for 3 h. After this the membranes were imaged in light microscope.

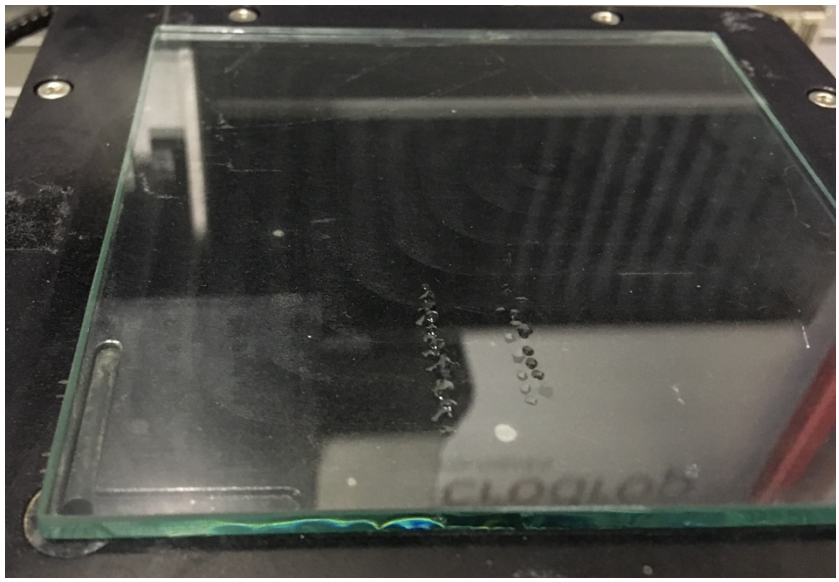

Figure 7 - Water line pattern above a glass plate using Microdrop.

Source: By the author.

3.13 Photobiomodulation test

The HFF-1 cells were seeded with at the middle of wells of TCP with appropriate medium for 24 h and 5 % of CO_2. To perform the analyses, the cells were washed and incubated with PBS prior to irradiation. Each irradiation occurred with light fluence of 15J/cm^2 at 660 nm and with a gap of 1 h among them, after the cells

were imaged at light microscope and medium was restored. This experiment is intended to measure the mobility of cells and the growth. Finally, after 3 irradiation and 24 h later, the cells were assess through MTT test.

3.14 Statistical tests

The Kruskal-Wallis test was performed to analyze the population distributions of cell's circularity and cell's aspect ratio, which do not necessarily assume normal distribution. Wilcox test paired the groups to identify possible differences among groups. The experiment of cell attachment was tested with Anova 1-way to analyze the means. Tests of normal distribution were performed to confirm the distribution. Analysis were made by R Statistics Software.

4 RESULTS AND DISCUSSION

4.1 Synthesis and H- and C13-NMR characterization

Four different chitosan were synthesized with the positive ammonium group (QCh), they were obtained from a chitosan (Ch) with 77.9% of deacetylation and 600 kDa. The degree of deacetylation is presented in Table 1, which is in proportion to GlcN and GlcNAc monomers at the polymer. All four groups presented a deacetylation degree around 77% for all chitosan derivatives. Then there are more units of GlcN at the polymer, although authors classify chitosan differently (44, 45), this high degree of deacetylation is considered chitosan by all. The molecular weight determined by viscometer is presented in Table 1. There are two derivatives with a molecular weight around 1000 kDa and other two around 400 kDa, it is important to acknowledge here the studies consider a higher molecular weight between 300 ~ 400 kDa (46-47), which is our lowest molecular weight obtained through the process.

Table 1 - Deacetylation degree of chitosan compounds measured by H-NMR.

	Deacetylation (%)	Molecular weight (kg/mol)
Chitosan	77.9 ±1.9	600
8% DQ and LMW	76.8 ± 0.1	426
8% DQ and HMW	76.8 ± 0.1	985
40% DQ and LMW	78 ± 1.1	380
40% DQ and HMW	78 ± 1.1	960

Source: By the author.

The synthesis of quaternized chitosan derivatives yields four white powders with 2 different DQ and 4 molecular weights. The groups were chosen to have high or low DQ and high or low MW. The chemical shift of H1 changed through the samples, as expected, and there is a decreased peak area at H1 (4.8 ppm) and an increased peak at 5 ppm at substituted samples (Figure 8 b,c) when compared with non-substituted chitosan (Figure 8 a) this demonstrate a reaction at the carbon chain. The substitution is believed to be N-substitution, because the reaction is performed in acid medium. (39, 48)

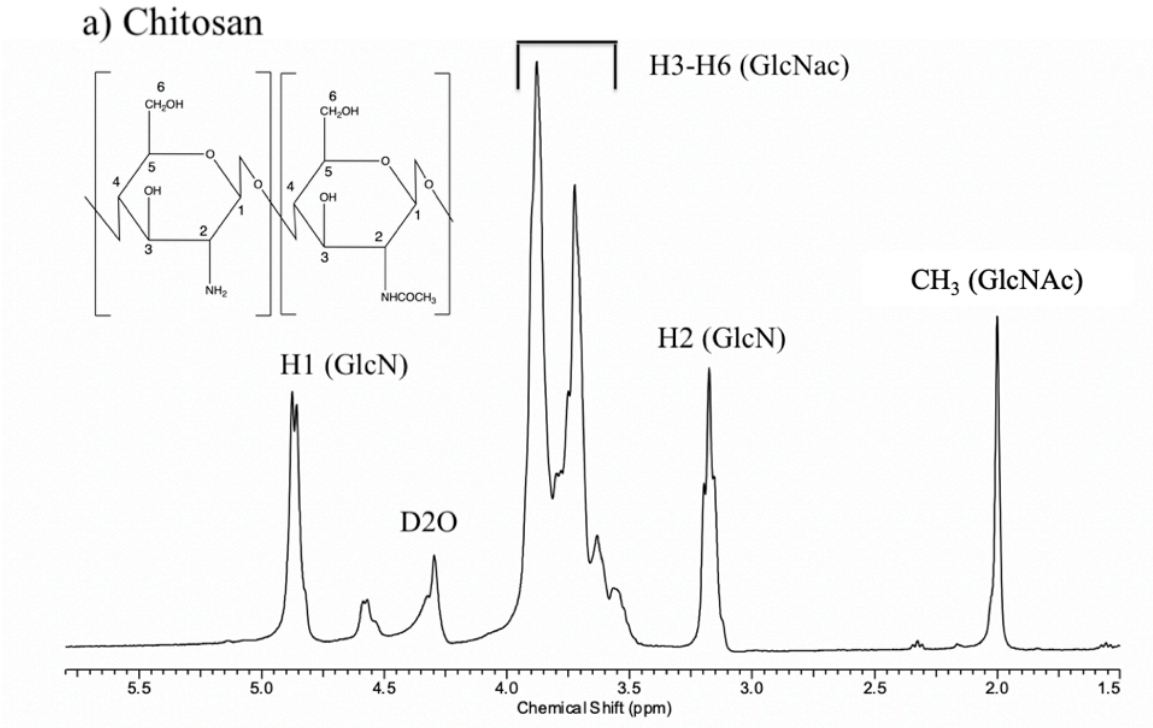

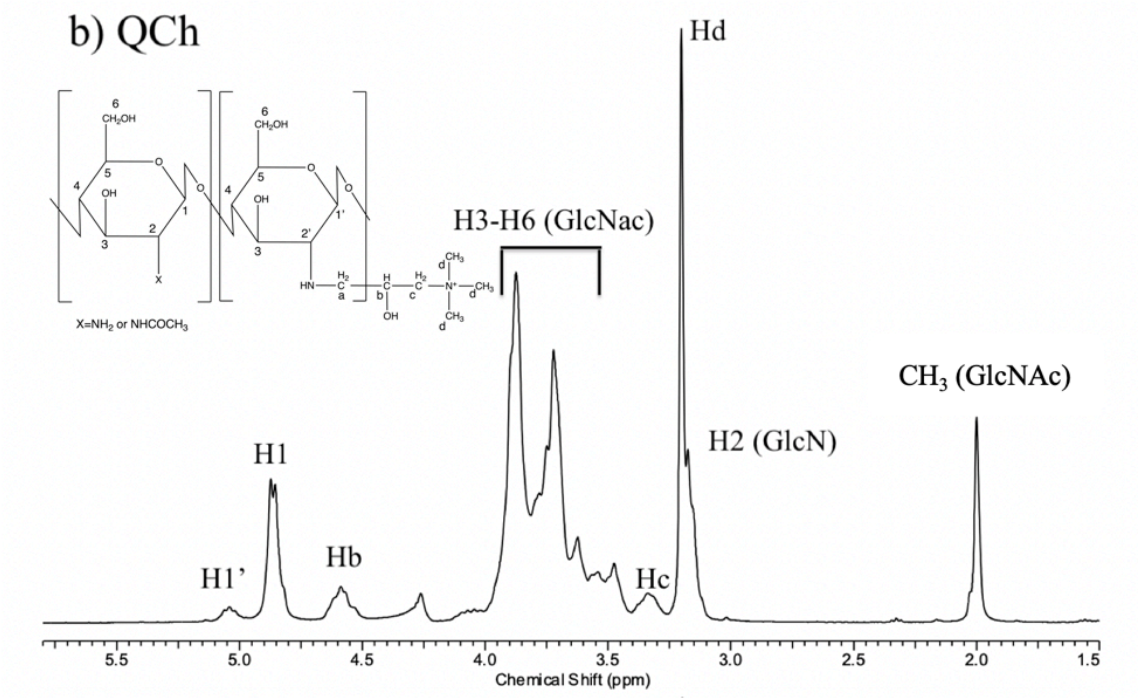

(to be continued)

(continuation)

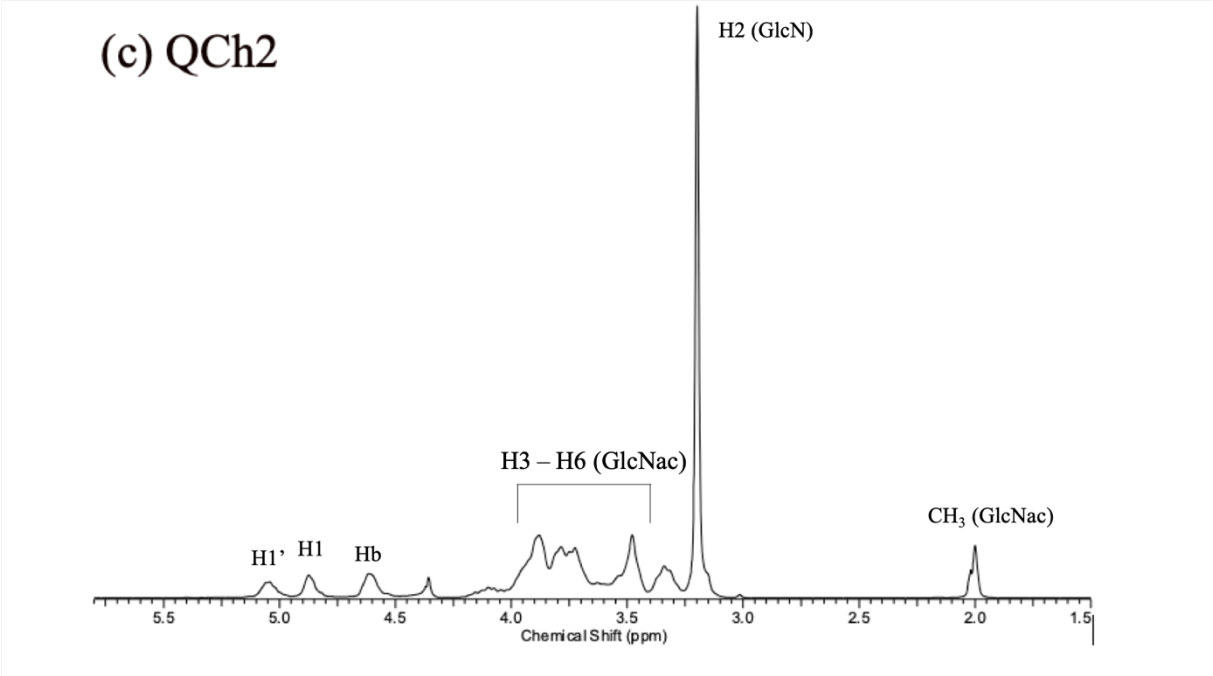

Figure 8 - H1 NMR spectra of a) chitosan, b) QCh1 low DQ and c) QCh2 high DQ in solution D2O/HCl 1% (v/v) acquired at 85 °C.

Source: By Dr. Danilo Martins dos Santos.

Titration was performed and presented similar results compared to H-NMR for the four synthetized chitosan derivatives (Table 2). These results indicate there are one and four monomers with ammonium group in every 10 monomers at, respectively, the lowest and the highest degree of quaternized chitosan derivatives. Also, they could reach values up to 70% DQ (39).

Chemical shifts of C13 NMR are presented in Table 2 with their respective integrated peak areas. The first line belongs to C13 from Chitosan, assignment by Domard, A. *et al*.(49) All the peaks were normalized according to the first carbon (C1), which is anomeric. The C_{13} is expected to be equally distributed in nature, so it is expected peaks areas around 1, since each position at the carbon chain does not have any advantage among others. The chitosan presented integrated carbon peaks around 1, but the derivatives groups presented different values of the integrated carbon peaks for C2, C3, C4, C5 and C6, which could be some evidence of another reaction site. The only notable and very different spectra was the 40% degree of quaternization, which presented new peaks between 70 and 60 ppm (Figure 10 and

Figure 11). Another hypothesis, the peaks changed because the new chemistry environment around these carbons. New experiments are necessary to clarify this hypothesis.

Table 2 - C13 NMR Chemical Shifts of Chitosan and derivatives with their respective Integrated Areas

	C1(ppm)	I_{C1}	C2(ppm)	I_{C2}	C3(ppm)	I_{C3}	C4(ppm)	I_{C4}	C5(ppm)	I_{C5}	C6(ppm)	I_{C6}	$(Me)_3N^+$(ppm)	$I_{(Me)3N+}$
Chitosan(49)	97.23		55.8		69.8		77.09		74.5		60.2			
Chitosan	98.97	1	56.75	1.15	71.35	1.01	78.09	1.02	75.35	1.13	60.62	1.28	-	-
10% DQ 426 (kg/mol)	98.96	1	56.74	1.05	71.35	0.84	78.12	0.75	75.51	1.11	61.11	1.23	55.06	0.48
10% DQ HMW	98.98	1	56.75	0.94	71.37	0.8	78.1	0.73	75.33	1.13	61.11	0.67	55.05	0.36
40% DQ LMW	103.36	1	57.38	0.31	70.25	0.58	79.47	1.29	75.45	1.97	61.22	0.31	55.06	2.05

Source: By the author.

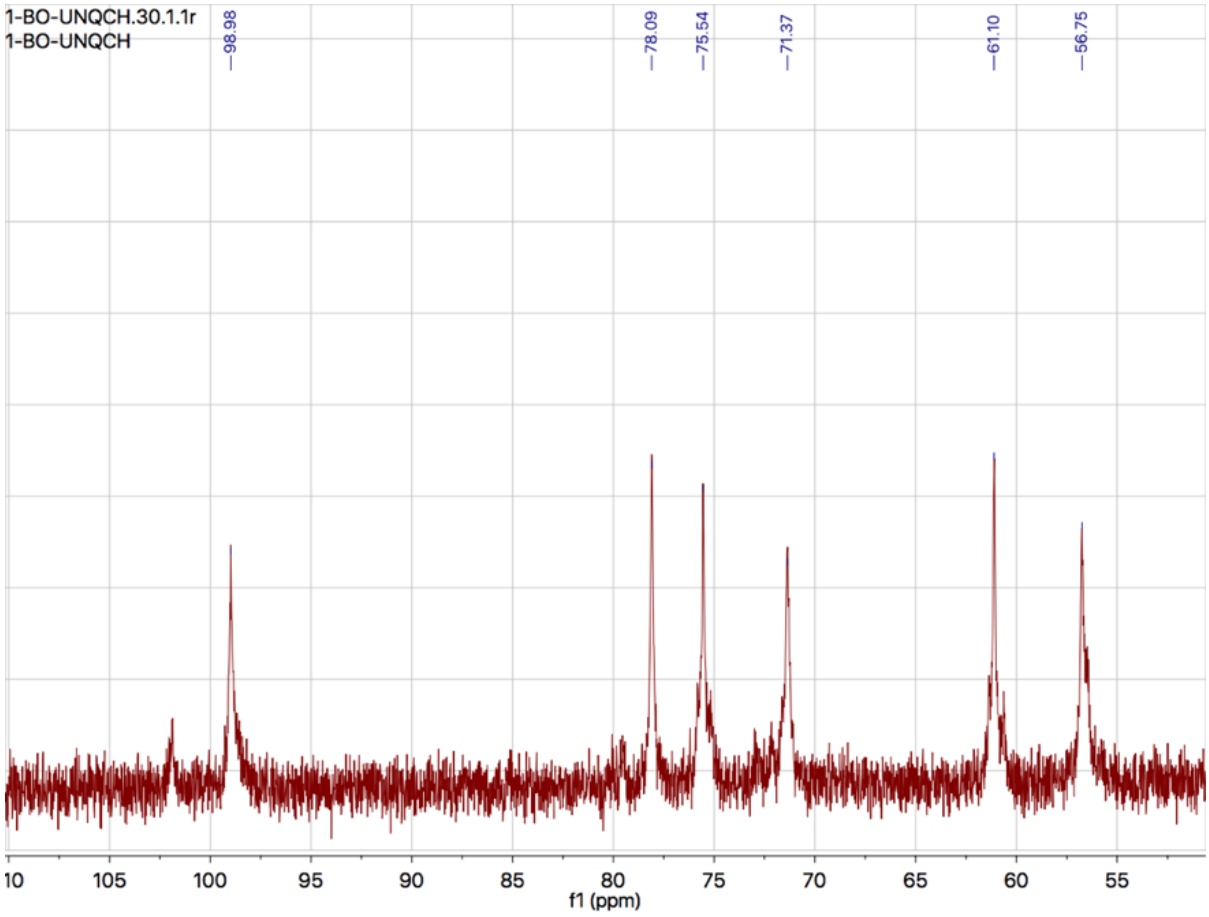

Figure 9 - C13 NMR Chitosan

Source: By the author.

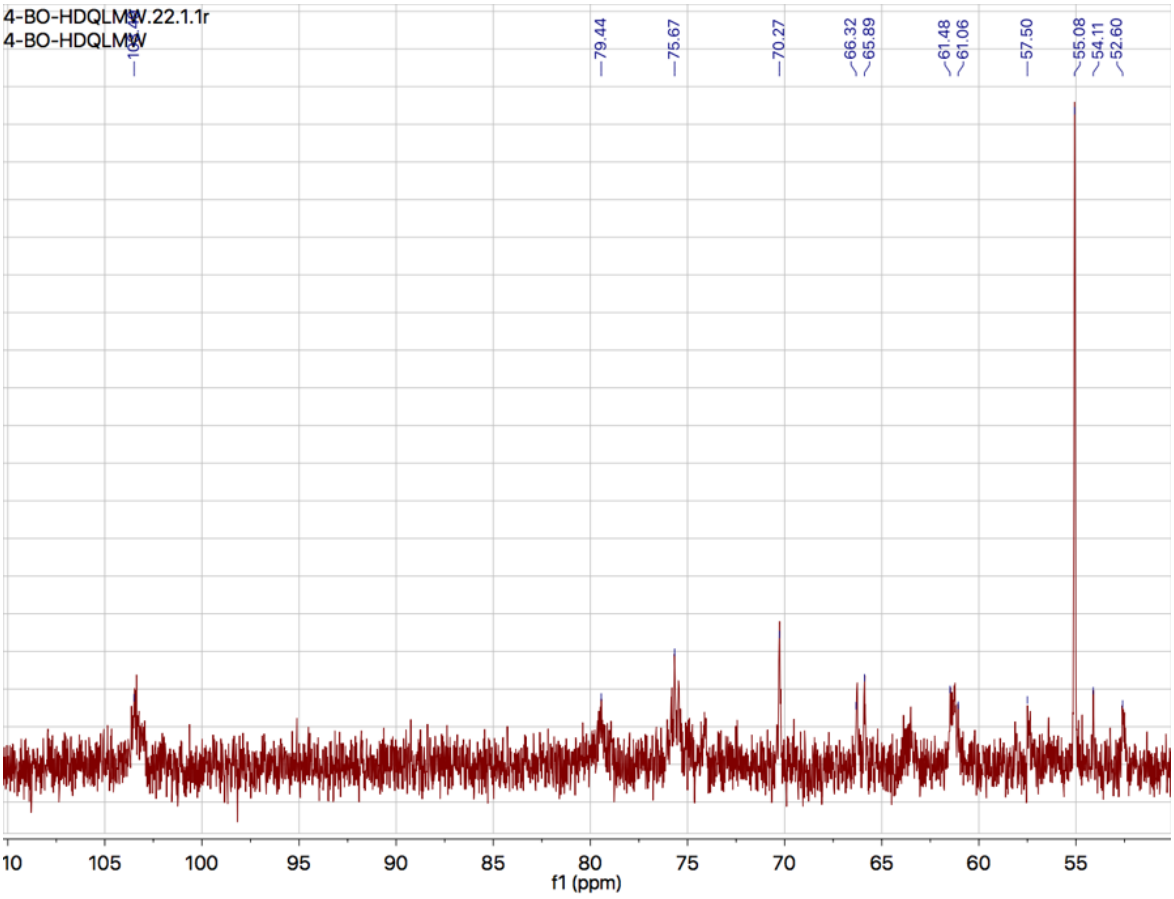

Figure 10 - C13 NMR spectra of 40% DQ QCh

Source: By the author.

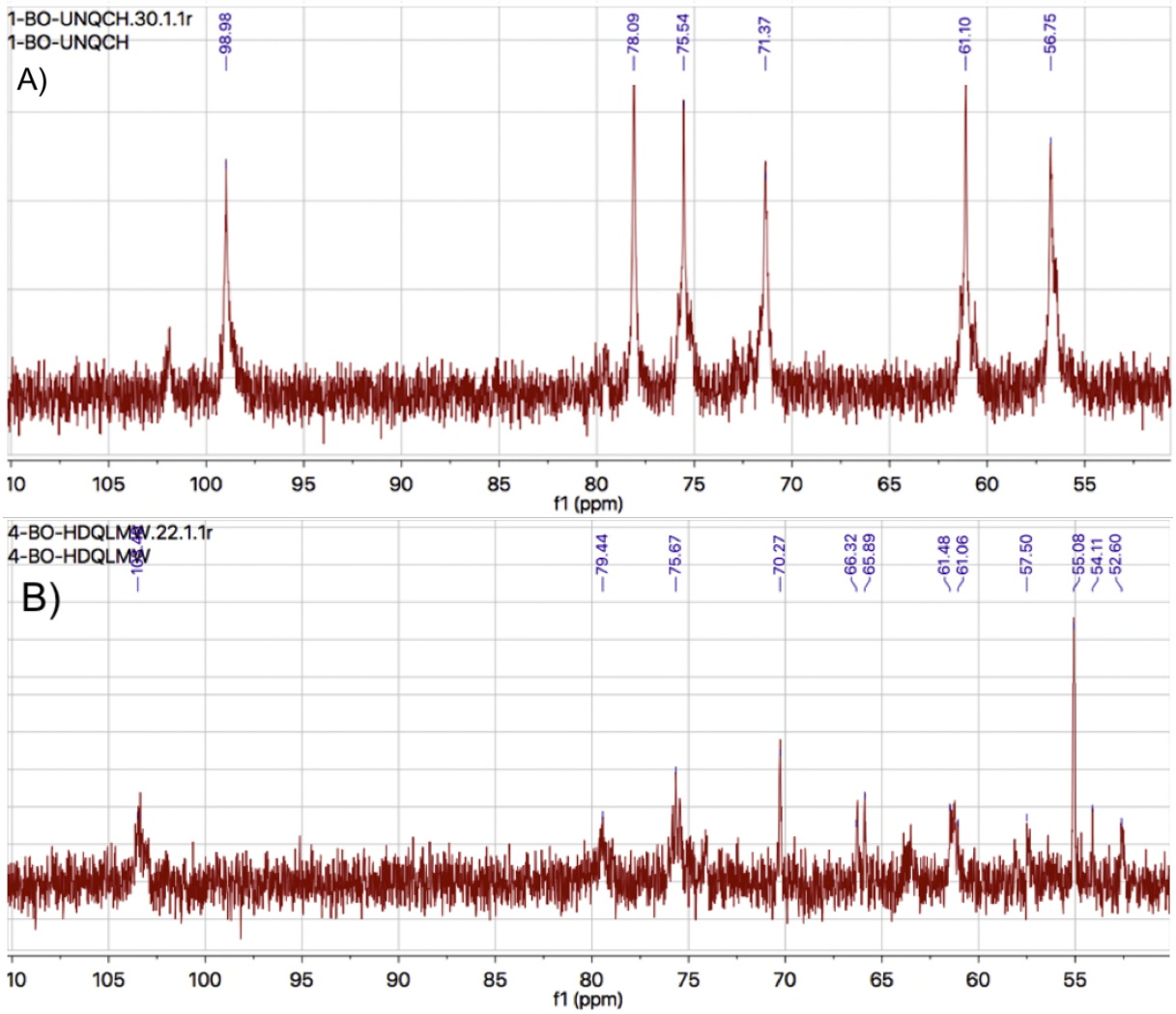

Figure 11-Stack of C13 NMR Spectra of A) Chitosan and B) 40% DQ Chitosan derivative

Source: By the author.

Table 3 - Quaternization Degree

Groups	H NMR DQ = $I_{H1'}$/ ($I_{H1'}$ + I_{H1})*100	Titration
LDQ LMW	8,2 ± 1,5	9.9 ± 0.4
LDQ HMW	8,2 ± 1,5	9.9 ± 0.4
HDQ LMW	41,3 ± 2,2	34.9 ± 0.2
HDQ HMW	41,3 ± 2,1	34.9 ± 0.2

Source: By the author.

4.2 Surface characterization: Capacitive Coupling (dC/dz)

The measurement of dC/dz by the AFM tip close to a surface is proportional to the surface charge amount probed by the tip. The hydrogel surface casted with 9% and 40% DQ QCh presented, respectively, 1.3- and 2-times better charge mobility than chitosan observed at distribution of capacitive coupling (Figure 12). Cationic cellulose synthetized with GTMAC presented similar results compared with 40% DQ QCh casted above cellulose. (10)

These charges seem to modify different sites above the material in response to the object's proximity. Then it is expected, the plasmatic membrane induces rearrangement of charges at the surface membrane that results in a better cell adhesion. The attraction of positively charged surface and plasmatic cells membrane is another influence to a better interaction. (50)

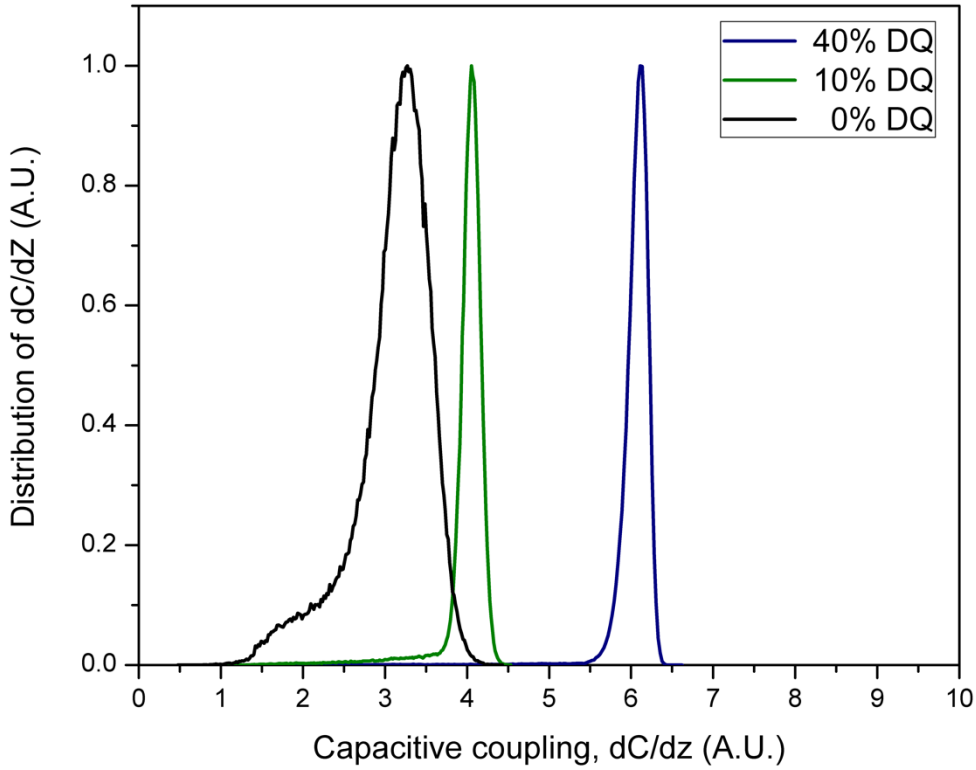

Figure 12 - Capacitive coupling distribution for hydrogels with casted chitosan derivates and chitosan. A) Black: hydrogel casted with 0 % DQ chitosan, B) Green line: hydrogel casted with 10 % DQ chitosan derivative and C) Blue Line: hydrogel casted with 40 % DQ chitosan derivative.

Source: By the author.

The hydrogels casted with 40 %, 9 % and 0 % DQ chitosan derivatives presented average roughness of, respectively, 25 ± 6 nm (40%), 30 ± 7 nm (9%) e 200 ± 82nm Ch (Figure 13A-C). This last has the highest average height among the other. It appears that chitosan fills in the surface structure that generate the primary roughness of the hydrogel in order to obtain a smoother surface for the chitosan/cellulose system. Although, the surface roughness proved to be a considerable factor for cell attachment (51-52), the next experiments will show the importance of cationic surface modification at cell attachment.

The samples images given by the Capacitive Coupling technique (Figure 14) showed black spots that represent insulating regions, where the charge induction is poor. The white regions, which represent a better induction sites that are homogeneously distributed throughout the entire hydrogel casted with 40% DQ chitosan derivative (Figure 14A). On the other hand, hydrogels casted with chitosan

and 10% DQ chitosan derivative presented highly insulating regions observed by black/white surface constrast (Figure 14B-C).

Since the hydrogels are very moist in contact with the cells through the medium, we tested the influence of the water vapor above the material injecting it into the chamber. The same material presented capacitive coupling dependence for different humidity environment percentages. The material became insulating as the water vapor decreases inside the chamber. In this context, the material has a dependence on water to become more inductive. This presents a possible explanation for how cells could induces charges in aqueous solution when they are approaching the material surface.

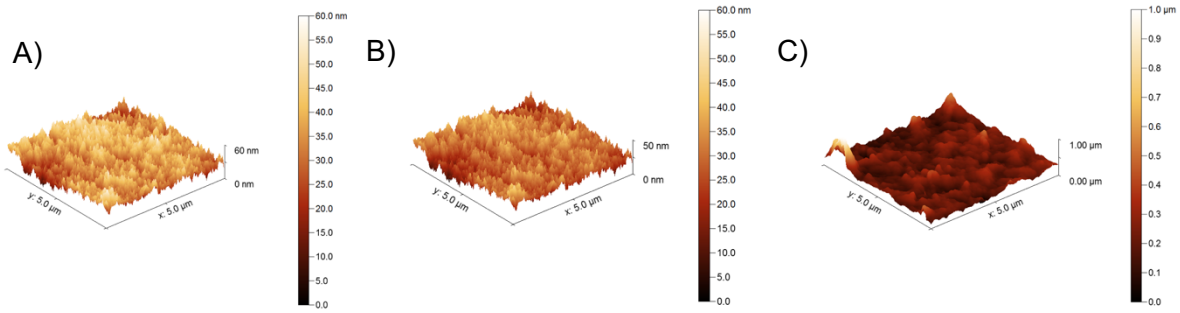

Figure 13 - AFM topography of hydrogels casted with: A) 40% of quaternized chitosan (60 nm scale), B) 10 % DQ QCh (60 nm scale) and C) Chitosan (1 µm scale).

Source: By the author.

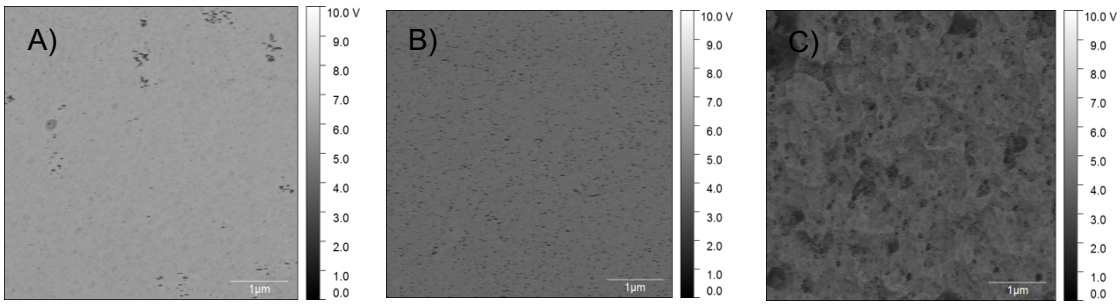

Figure 14 - Capacitive coupling topography of hydrogels casted with: a) 40% DQ QCh, b) 10% DQ QCh and c) chitosan. White regions are less insulating than black ones.

Source: By the author.

4.3 Ninhydrin adsorption and FT-IR

The interaction between the chitosan and cellulose was first observed through the well-known Ninhydrin reaction. The reaction evidenced a purple color in the hydrogel (Figure 15). This indicates a reaction with the primary amino group of chitosan (GlcN), since cellulose does not have amino groups.

Figure 15 - Hydrogel of cellulose casted with chitosan reacted with ninhydrin. The purple color at the edges indicates the interaction between chitosan and cellulose.

Source: By the author.

The FT-IR was performed for powders of chitosan derivatives and for hydrogel and chitosan powders. The quaternized chitosan powders presented a better signal of the quaternized group at 1479 cm^{-1}, as expected, the ones with a higher degree of quaternization presented a low transmittance at this wavenumber. On the other hand, this signal group is not easily distinguished in hydrogels, which could be related to the penetration amount in the hydrogel (Figure 16).

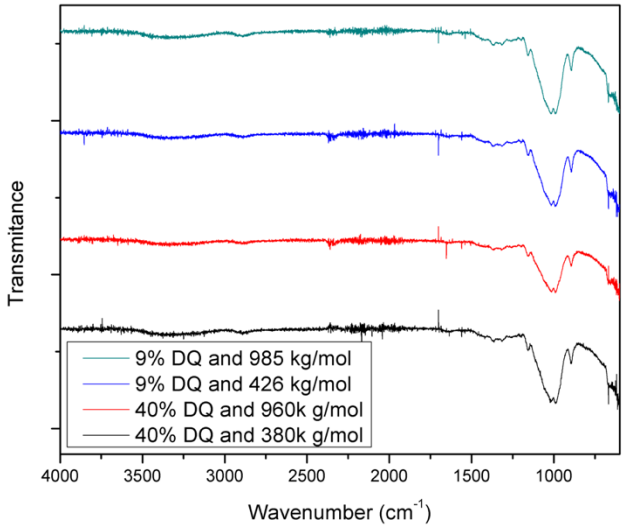

Figure 16 - FT-IR Transmittance of Hydrogels casted with Chitosan derivatives with different degrees of quaternization and molecular weight. The offset was applied to see all compounds.

Source: By the author.

The analysis was performed between 1400 and 1800 cm^{-1} due to equal and unique peaks for each compound (Table 4). Common peaks for chitosan at 1420, 1650 and 1786 cm^{-1} appeared for all groups. The chitosan derivatives appeared a new vibration due to ammonium quaternary group. Some researchers observed this group at 1475 cm^{-1} or 1483 cm^{-1}, in our experiments the decreased transmittance at powder chitosan appeared in 1479 cm^{-1} and 1477 cm^{-1} for, respectively, 40% and 9% DQ. (53, 54). Different from powder, the hydrogel casted with modified chitosan did not presented a decrease peak at 1479 cm^{-1}, which is easily seen superposing the spectra of casted hydrogel (Data not shown) and this probably explained at next experiments, where we found the QCh at the hydrogel's surface.

Table 4 - Comparison peaks between 1400 and 1800 cm^{-1} for chitosan derivatives powder.

Functional Group	Chitosan	9% DQ	40% DQ
C-H/O-H	1418	1420	1420
C-H	1470		
$^{+}N(CH_3)_3$	-	1477	1479
Amide II	1568	-	1560
NH_2	1610	1610	-
N-H	1651	1653	1654
C=N	1786	-	1787

Source: By the author.

There is an increasing peak transmittance at 1610 cm^{-1} for powders with 40% DQ, this peak is related to the vibration of NH_2 (55) (Figure 17).

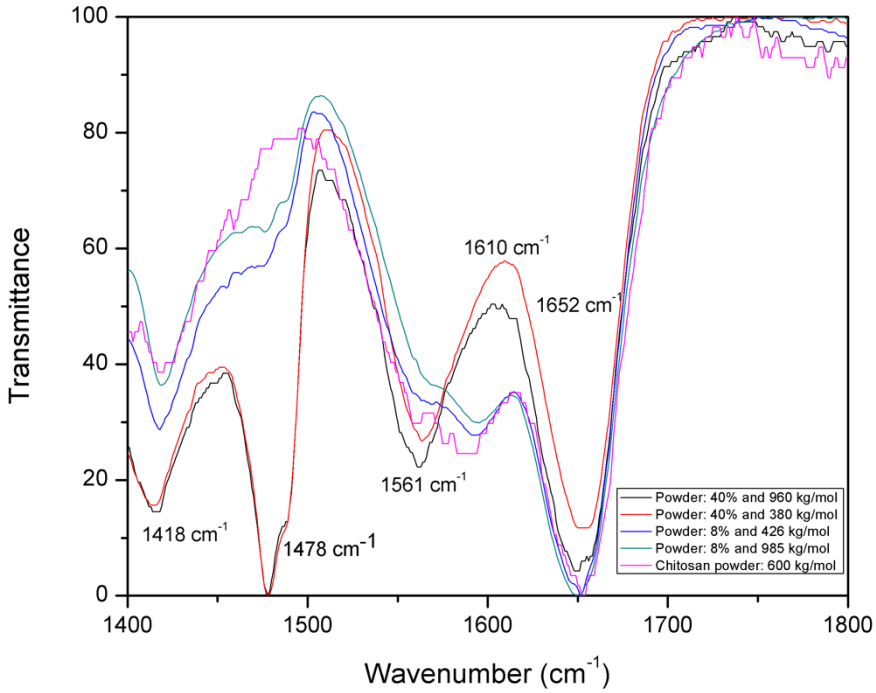

Figure 17 - FT-IR of quaternized chitosan derivatives powders for a normalized transmittance.

Source: By the author.

4.4 The fluorescence of chitosan, chitosan derivates and hydrogels

Before considering the emission properties of hydrogel/chitosan based films, it is important to analyze the stability of chitosan in the aqueous medium, since the material is stored in PBS buffer solution containing Sodium Azide 0.1% (wt). Here, the supernatant of stock hydrogel solution was analyzed by two techniques, in which one the fluorescence of hydrogel/chitosan films was analyzed by confocal microscopy using two-photons (2P) excitation at 800 nm and by absorbance spectrum using UV-Vis spectroscopy. The supernatant of the hydrogel storage solution (blue, green, magenta and yellow lines) was analyzed by UV-Vis Technique (Figure 18) by comparing with new fresh control solutions of only 40% DQ quaternized chitosan (0.1% wt, black and red lines) without Sodium Azide, of pure Sodium Azide (0.1% wt, dark red line) and of chitosan containing Sodium Azide (nave blue line). The baseline was made for Mili-Q water for all samples. The control solutions of only 40% DQ quaternized chitosan show broad absorption band that extend from the UV to the visible range. The absorbance spectra tails have similar traces between the control and the quaternized chitosan solutions.

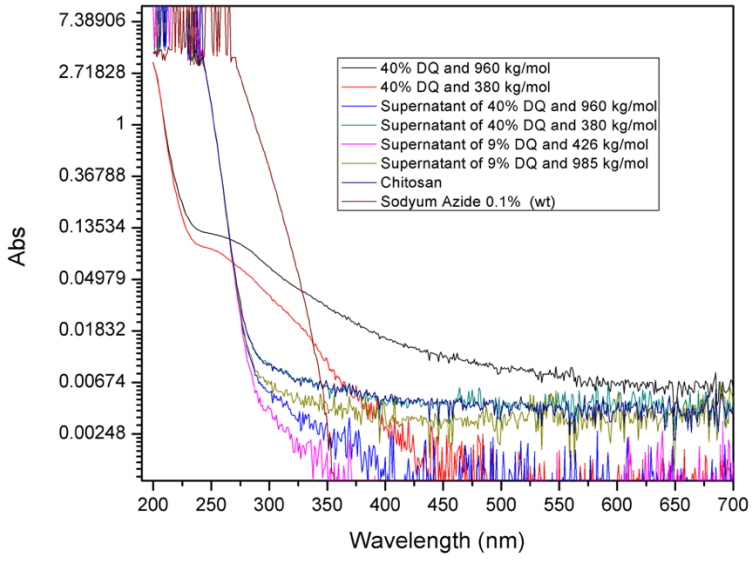

Figure 18 - UV-Vis measurement of High Quaternization Degree of Chitosan solutions 0.1 % (wt) and supernatant of hydrogels storage solution.

Source: By the author.

However, the supernatant spectrum shows only traces of chitosan in the storage solution of Sodium Azide 0.01% (wt) superimposed by an absorption onset below

270 nm due to the Sodium Azide. This result demonstrates structural and chemical stability in aqueous media of both chitosan and hydrogel matrix.

The normalized fluorescence spectra from chitosan derivatives powders Figure 19 has peaks at 470, 495 and 660 nm. The peak at 495 nm seems to increase with the degree of quaternization. Lambda mode was used to acquire the spectra through the confocal planes of the hydrogels.

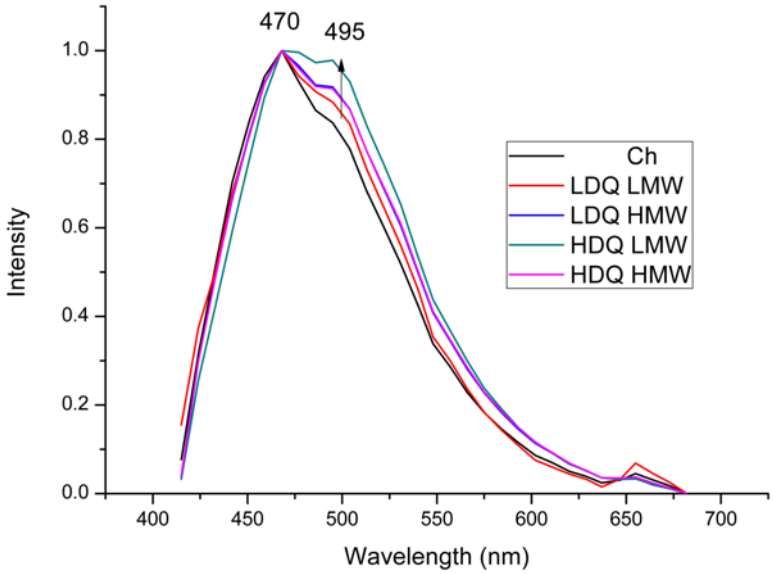

Figure 19 - Fluorescence spectra of chitosan powder derivatives recorded at confocal microscopy.

Source: By the author.

The confocal planes associated to the bottom, middle and top positions of the hydrogel were selected. The bottom and top confocal images of the hydrogel are presented in (Figure 20) as well as the fluorescence spectra that were evaluated at different region of interest (colored circles and squares). Pieces of the hydrogel/chitosan-based films were deposited on glass slides and analyzed in aqueous PBS solution to ensure the perfect parallel alignment with the scan plane necessary for the confocal characterization in this work. The image of the surface (top) of the film shows a bluish violet color associated with bright emission of chitosan evaluated at the edge (black circle) and along the upper surface (red circle) with a maximum at 443 nm. The PBS solution (blue circle) shows no traces of chitosan emission, indicating a stable interaction of this molecule with the hydrogel in aqueous solution. Chitosan remains at the edge (black square) for the confocal plane image

positioned in the middle of the film, but it does not penetrate to the position of the region of interest given by the red circle. On the other hand, this region in the interior of the film has a weak emission in the green spectral range with a maximum around 500 nm, originating from traces of molecular impurities found in the cellulosic starting material. Since the chitosan and cellulose has different fluorescence peaks, the chitosan penetration was measured through the hydrogel.

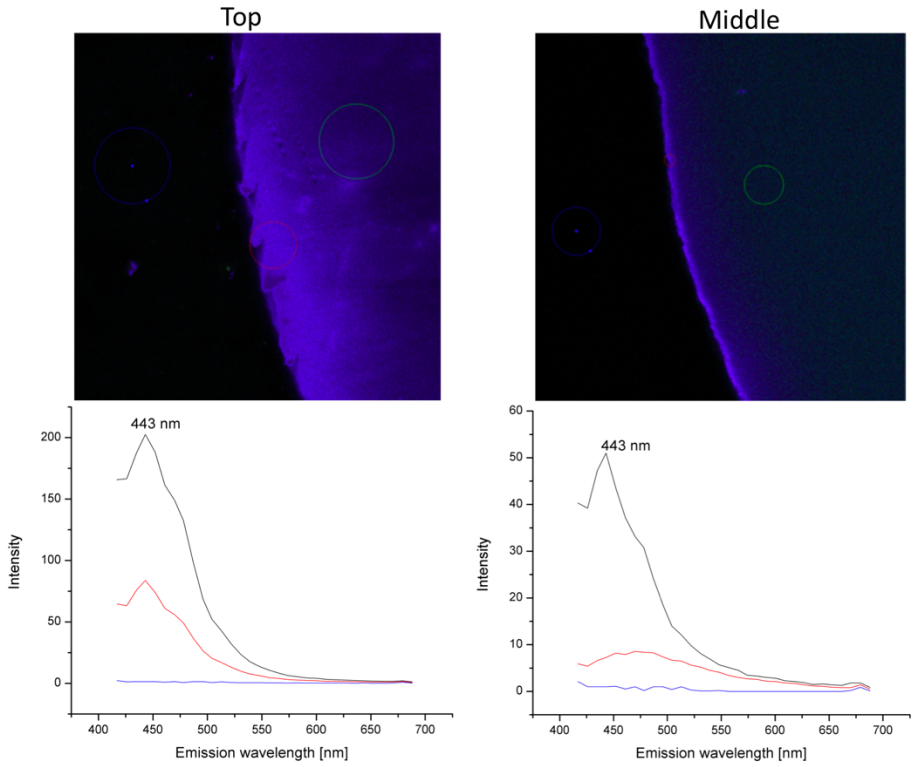

Figure 20 - Confocal microscope images of top and middle of hydrogels with their respective fluorescence spectrum. Three regions of interest were drawn in each image at the surface, border and outside of hydrogel. The black, red and blue lines at the spectrum rep.

Source: By the author.

As the hydrogel is porous, it is important to characterize in detail the interaction and permeation of chitosan in this matrix. Confocal microscopy allows assessing the degree of chitosan penetration into the hydrogel within the limits of an optical resolution of approximately 200 nm, since the emission spectra of cellulose in the matrix and chitosan are different. The chitosan penetration profile was spectrally evaluated in seven regions of interest (colored circles) along the spectral image of a confocal plane in the middle of the hydrogel in the region close to its edge (Figure 21a). The separation between the circles near the edge is 6 μm. The spectra

evaluated in each circle are shown in Figure 21b. The sample was excited by two photons at 800 nm. It can be seen that the spectral intensity drops considerably as we penetrate inside the hydrogel. Figure 21c compares the normalized spectra evaluated near the surface (red circle) and in the region furthest from the surface (blue circle) that correspond to the most intense emission of chitosan with a peak at 443 nm and the much less intense emission of cellulose in the hydrogel around 500 nm. The emission intensity of chitosan is 13 times more intense than that of cellulose at 443 nm at the surface. Hence chitosan can be distinguished from cellulose both by emission intensity or spectral position. Therefore, the chitosan penetration profile can be evaluated in the vicinity of the hydrogel surface. Figure 21d shows the image of the same confocal plane for chitosan emission at 443 nm and the red line for which the emission profile was evaluated (Figure 21e). Chitosan emission is 78% more intense in a region of 3 micrometers close to the edge, indicating a strong interaction of this molecule with the porous wall of the hydrogel.

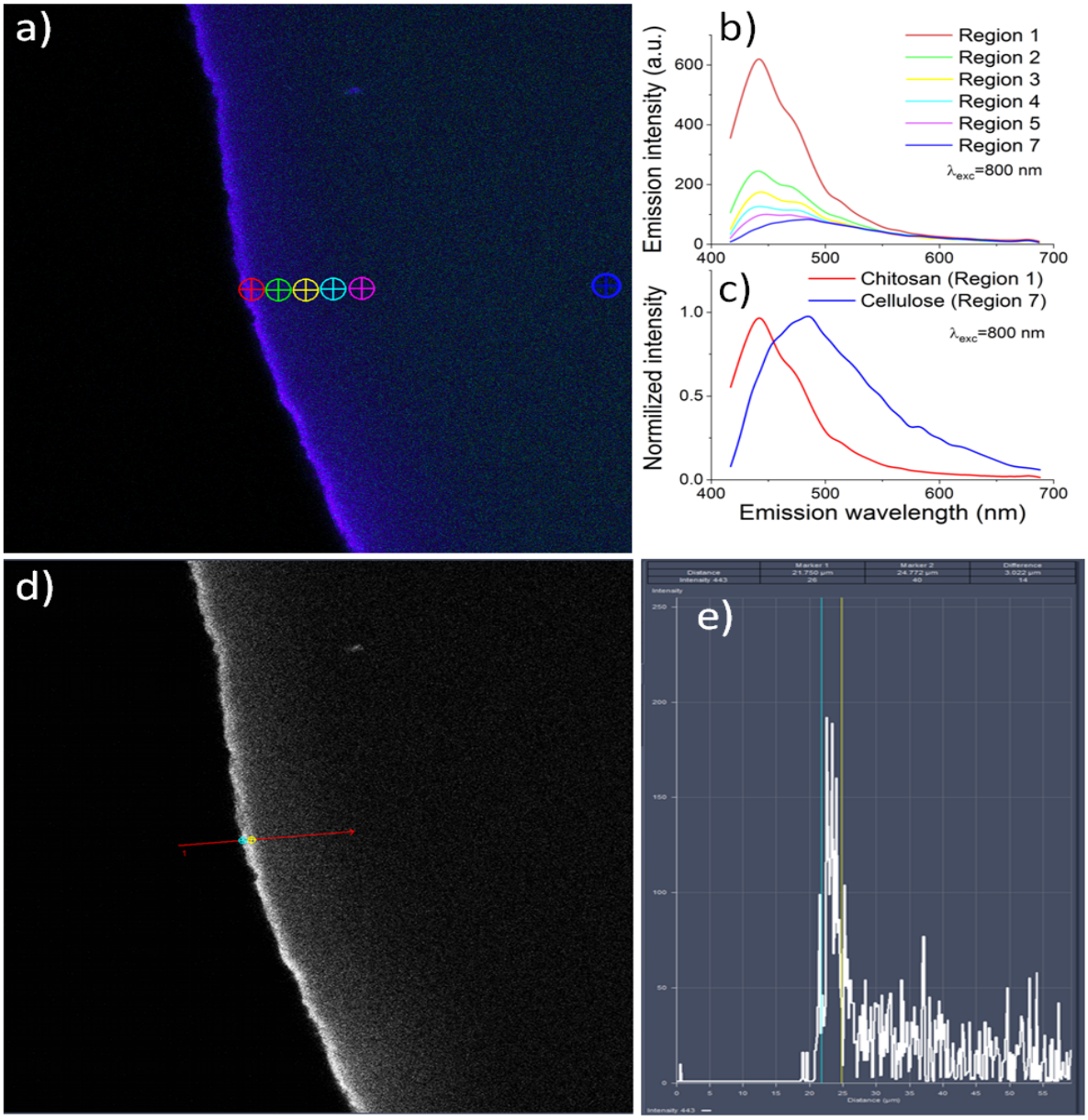

Figure 21 - a) Evaluation of chitosan penetration profile in seven regions of interest (colored circles) along the spectral image of a confocal plane in the middle of the hydrogel in the region close to its edge. b) Evaluated spectra for each region of interest. c) Normalized spectra evaluated near the surface (red circle) and in the region furthest from the surface (blue circle). d) Image of the same confocal plane for chitosan emission at 443 nm and e) the red line for which the emission profile was evaluated.

Source: By the author.

The emission properties presented above were used to structurally characterize the hydrogels studied in this work by confocal microscopy in channel mode. In this case, chitosan emission between 417-443 nm was measured in channel 1 (false color in blue) and that of cellulose between 550-700 nm was detected in channel 2 (false color in green).

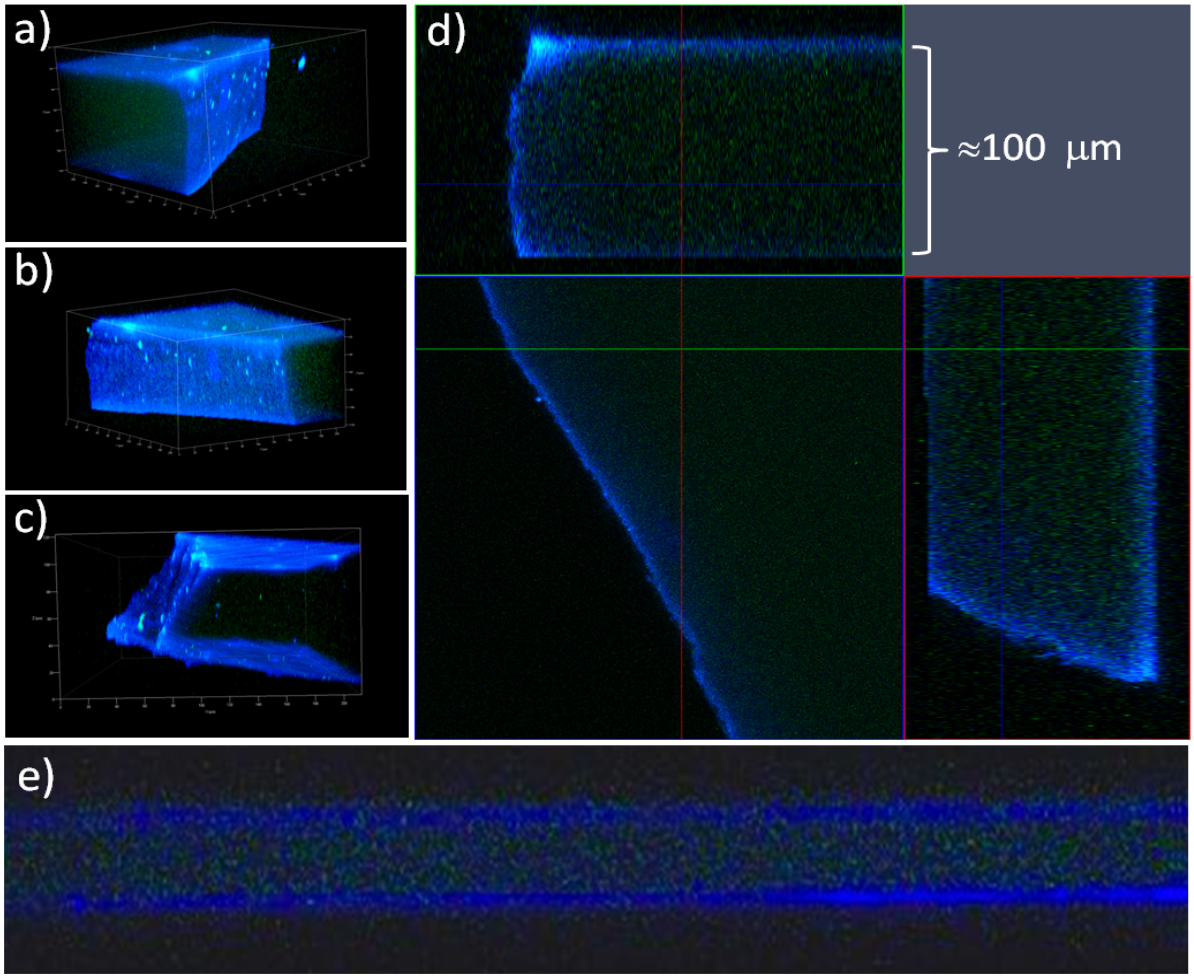

Figure 22 - a), b) and c) High contrast 3D (z-stacking) images with different spatial orientations of cellulose and chitosan hydrogel. The brighter blue false color represents the chitosan and the green color represents the cellulose. d) Image of a confocal plane

Source: By the author.

High contrast 3D (z-stacking) images with different spatial orientations of a chitosan-containing hydrogel film are shown in Figure 22 a, b and c. It is important to note that the hydrogels were measured in a wet condition. Therefore, they accumulate water in the pores inside and swell, while preserving the geometry due to the internal hydrostatic pressure in balance with the external hydrostatic pressure. These images show that chitosan covers the hydrogel film evenly. Figure 22 d shows the image of a confocal plane at the height of the blue line and the respective images of the orthogonal transverse planes taken along the green and red lines and shown on the sides to the right and above. Figure 22 e represents a cross-section in a region away from the edge of the hydrogel. It is important to note the great uniformity of the hydrogel thickness and the chitosan penetration profile throughout the entire sample.

The average thickness of hydrogels is approximately 100 µm (Figure 22 d) after the casting process and the penetration of casted chitosan inside the hydrogel is seen in the Table 5. Although there is little difference, the molecular weight seems to penetrate more with the decrease of polymer chain as expected.

Table 5 - Casted Chitosan penetration at the hydrogel

Chitosan Derivatives	Penetration (µm)
0% DQ and 600 kg/mol (Chitosan)	12
8% DQ and 426 kg/mol	12
8% DQ and 985 kg/mol	8
40% DQ and 380 kg/mol	14
40% DQ and 960 kg/mol	8

Source: By the author

4.5 Cell Attachment assay

This is the first experiment to observe an interaction with the mammalian cells. The number of cells was counted by the number of fluorescence nucleus stained by DAPI. The images of cell's nucleus fluorescence acquired started to evidence the difference among the hydrogels observed at Figure 23 by confocal microscopy and image analysis. Hydrogels casted with 40% DQ QCh had the most cell attach to it compared with the other membranes and some of the images showed similar results to TCP plate. This is the first evidence that positive charge seems to have an important effect on mammalian cells when occurs the interaction. The results were more obvious when we compared hydrogels casted with Ch, 40% DQ QCh and TCP plate seeing in Figure 24. TCP plate and membranes with high positive charge had micro identical regions, although this membrane had more blank spaces among cells than TCP. These results agrees with literature since there are reports showing the attraction of positively charged surface and plasmatic cells membrane. (56-57)

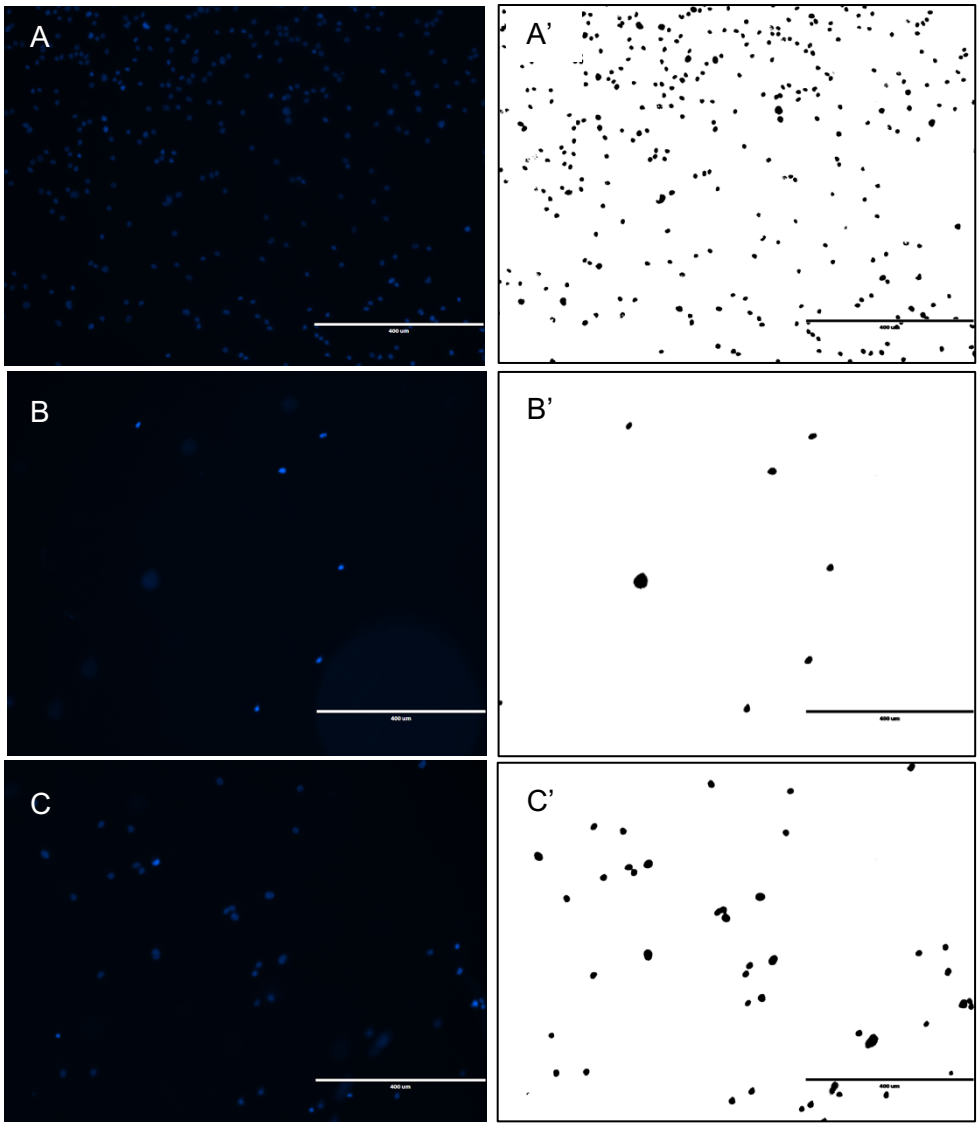

Figure 23 - Image of cell's nucleus fluorescence with and without treatment above: A and A') TCP, B and B') Hydrogel casted with Ch, C and C') hydrogel casted with 40 % DQ QCh.

Source: By the author.

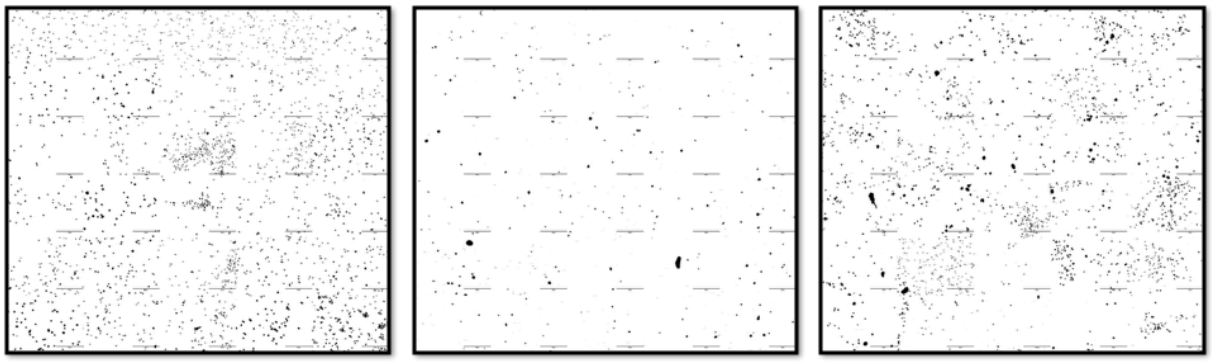

Figure 24 - Each black spot represents the nucleus fluorescence for one MG-63 cell. The fluorescence images were stacked together for the following groups: a) Tissue culture plate (control), b) Hydrogel casted with chitosan and c) Hydrogel casted with 40% DQ chitosan

Source: By the author.

The surface charges are important, but the fetal bovine serum (FBS) could be acting with the same role in TCP plate, where a layer of proteins coat the bottom and the cells start to bind to it. So, to prove our material is a ligand-free, the experiment was performed without FBS. The results are presented at Figure 25. The groups compared with tissue culture plate (TCP) presented for 40% DQ and 10% DQ, respectively, around 60% and 20% of cell attachment. The tissue culture plate control was hidden and correspond 100%. The parameters of FBS and molecular weight did not influence the cell's attachment, proving this material is ligand-free and do not need proteins binding to it. We also observed the growth factors are not important for the cell attachment, and the molecular size did not interfere too. The Anova test was performed to compare the means among groups with $p < 0.05$. The groups of hydrogels casted Chitosan and Low DQ Chitosan did not present significant difference between them, but there is significant difference among the groups with low and high DQ. The means were differentiate using Anova.

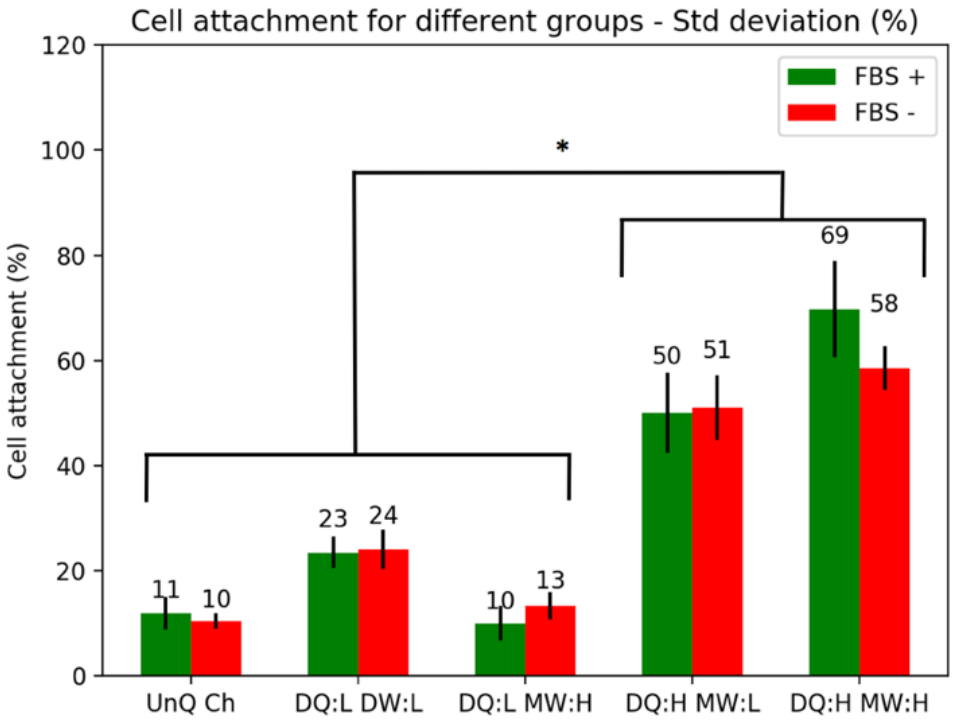

*Figure 25 - Percentage MG-83 attachment above cellulose hydrogel casted with different chitosan derivatives. The Anova test was performed to compare the means among groups * p < 0.05. The tissue culture plate control is hidden.*

Source: By the author.

4.6 The spreading assays

Another important parameter to be evaluated is the cell spreading. Cells without proper binding above the surface are an indicative they could not proliferate and a programmed death will be signalized. This measurement was made by calculating the circularity of the cells above the hydrogel using also fluorescence. Cell nuclei were labeled with DAPI emitting in blue and cytoskeleton were stained with a green fluorescent dye in order to capture cell shape. The images were recorded and the cell borders were treated as observed in Figure 26.

The results of circularity and aspect ratio are summarized at boxplot graphs (Figure 27 and Figure 28). The groups of High DQ and Tissue culture plate (TCP) presented similar median circularity. This lower number indicates cells with more spread and less round shape, while aspect ratio higher than one indicating also

spreading of cells and that the surface promote cell binding and mobility since cells are able to reach others and start to proliferate and grow. This is important characteristic for increasing cells number, since without the proper contact and binding with the material, the cells will not survive. Hydrogels with 10% DQ presented lower populations of spreading cells and they were more round shape. Similarly, the density charge affects more circularity than the molecular weight.

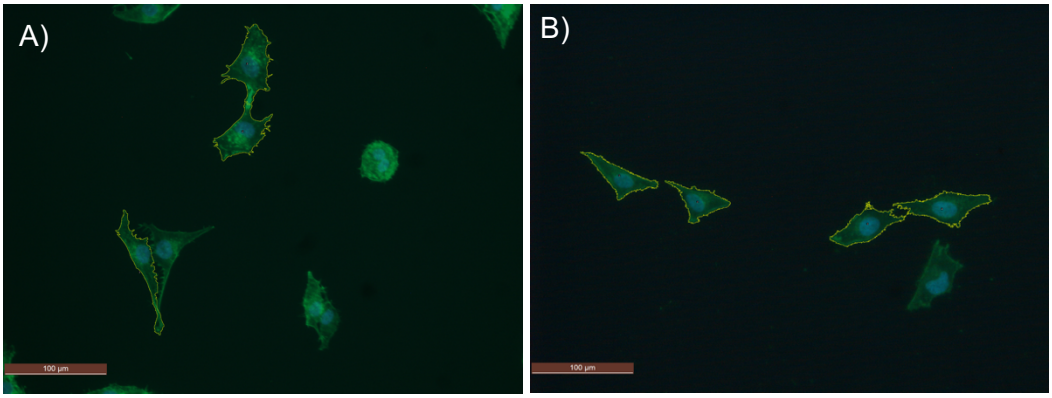

Figure 26 - Circularity measurement. The cells are above a) TCP and b) 40% DQ Chitosan

Source*:* By the author.

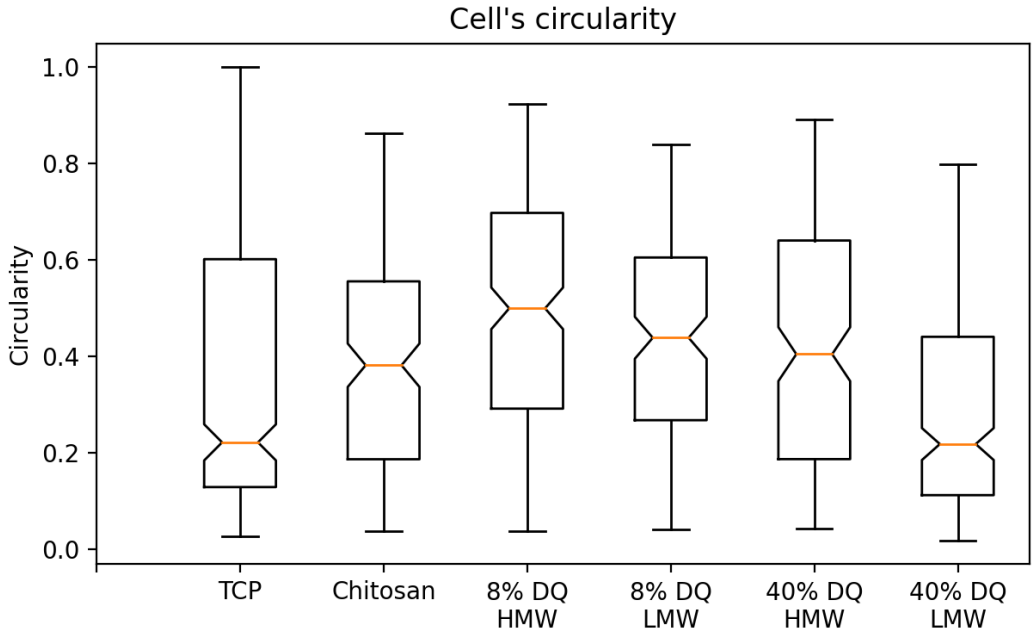

*Figure 27 - Cell's Circularity tested above cellulose hydrogels casted with different chitosan derivatives. Kruskal-Wallis test performed with * p < 0.05*

Source: By the author.

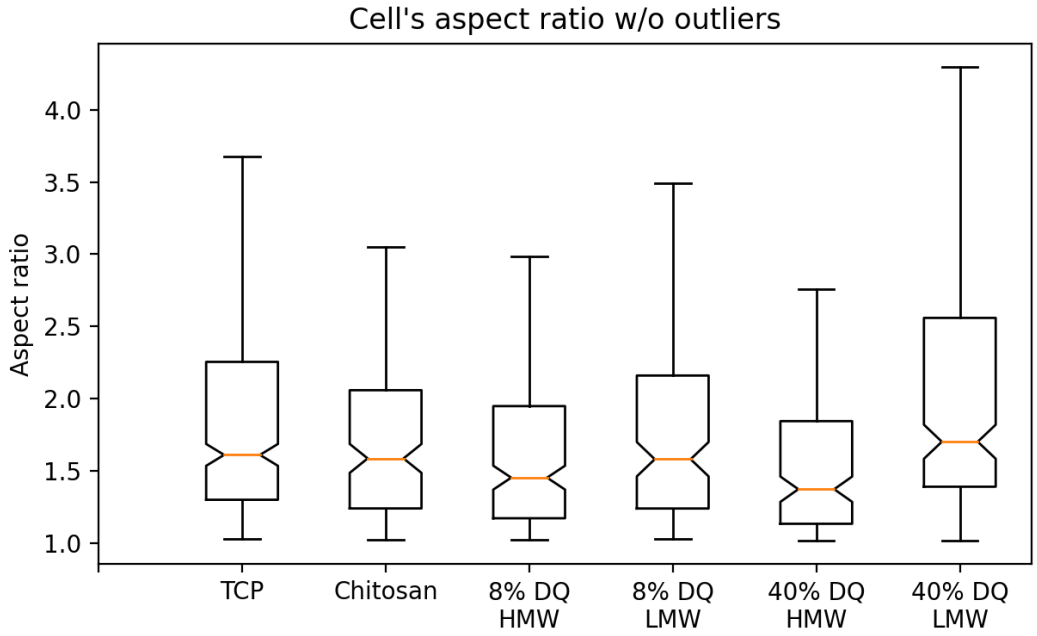

*Figure 28 - Cell's aspect ratio tested above cellulose hydrogels casted with different chitosan derivatives. Kruskal-Wallis test performed with * $p < 0.05$*

Source: By the author.

4.7 Cytotoxicity assay

MTT test will reveal metabolic activity of the cells above the hydrogel, since the attachment and spreading are not signal of healthy cells. The test measures the mitochondrial activity through the indirect reduction reaction of a yellow tetrazolium salt to a purple and insoluble salt called formazan.

At first, the results (Figure 29) of cytotoxicity for mammalian cells above the hydrogels appear to be high compared with TCP plate, which is considered as our 100% of viability. In the experiment, the absorbance of dilute formazan will be low compared to TCP control group since it is proportional to the number of cells above each surface considering our membranes as well as the TCP control. It is possible to see the low number of cells above the hydrogels (Figure 30) that reacted with MTT when imaging the wells with an Optical Microscope. There is significant difference between the groups of hydrogels with cells (blue bars) and the control group of TCP plate with cells (hidden from graph). The group control of hydrogels without cells did not react with the MTT reagent. Although, the higher DQ group is not presenting the

higher cell viability, all the cells above the membrane presented formazan inside the cell. All groups did not have significant differences among them.

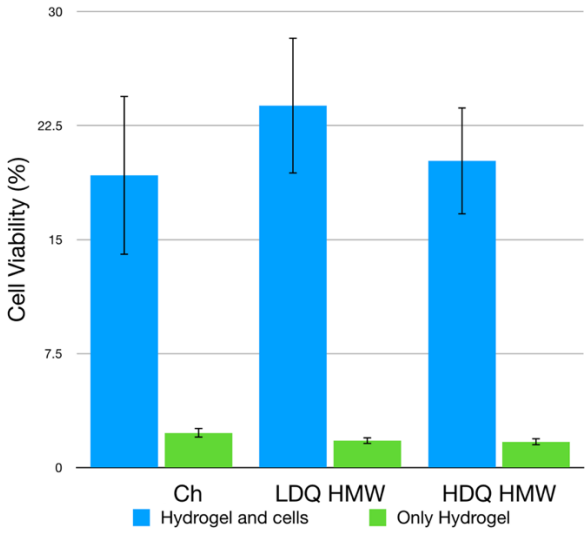

Figure 29 - Comparison of Cell viability for different hydrogels casted with chitosan (blue bars). The control without cell (green bars) is presented. There is significant difference among groups and tissue culture plates. The test was performed by the ANOVA method with $p<0.05$.

Source: By the author.

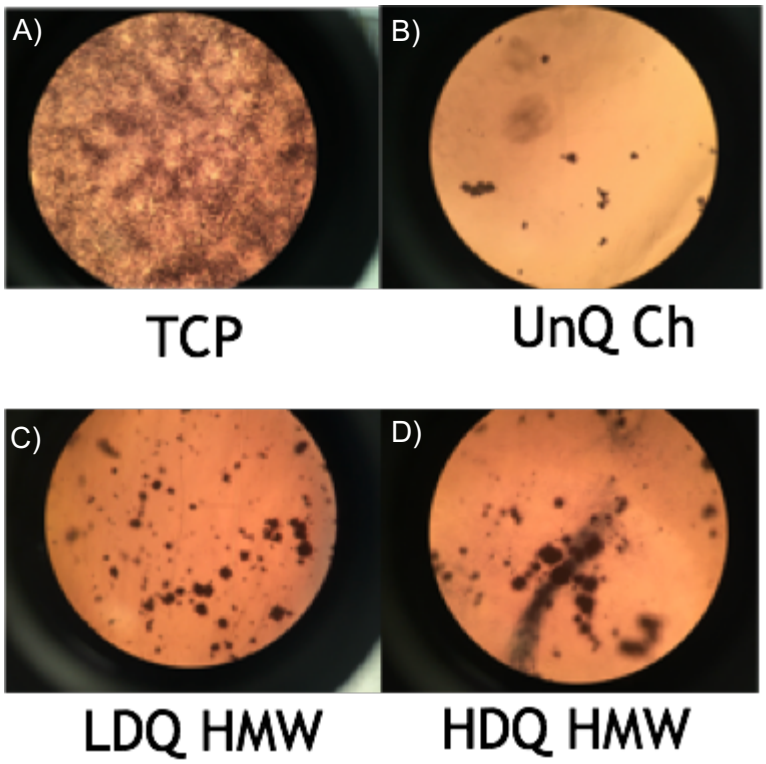

Figure 30 - MTT assay for MG-63 cells above hydrogel casted with chitosan. A) Tissue culture plate, B) chitosan, C) chitosan 9% DQ and D) chitosan 40% DQ.

Source: By the author.

The bacterial assay was performed for all DQ QCh membranes (Figure 31). The hydrogel with 40% DQ QCh presented a higher number of E. coli death (red ones) (Figure 31D) than the other groups. Although, the positive charge influences the cell death, this same group presented a higher number of not-death E. coli (green ones) above the hydrogel. The dead ones could be acting as a substrate to support the new bacteria.

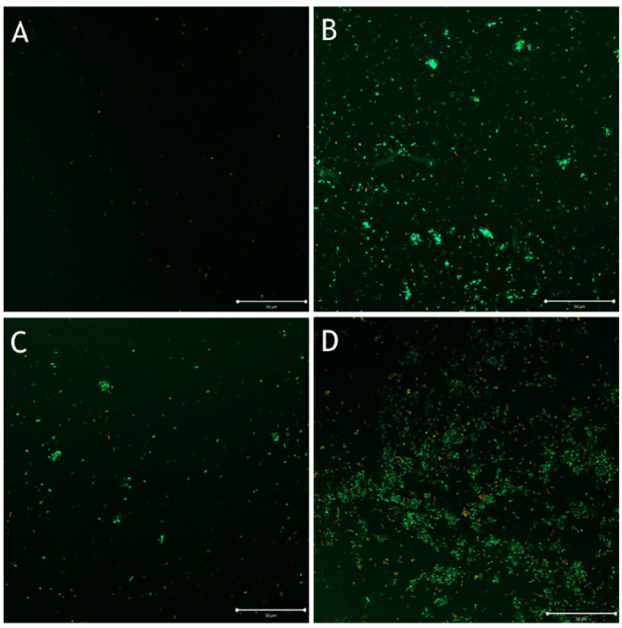

Figure 31 - Bacterial assay with gram-negative bacteria (E. coli) tested against cellulose hydrogel casted chitosan. A) Only cellulose, B) Chitosan, C) 9% DQ Chitosan and D) 40% DQ Chitosan. The higher dead cells presented at 40% DQ Chitosan, however this same group appeared a higher count of bacteria.

Source: By the author.

The number of dead cells per cm^2 is presented at Figure 32, which we could observe a greater difference among the groups without higher positive density charge.

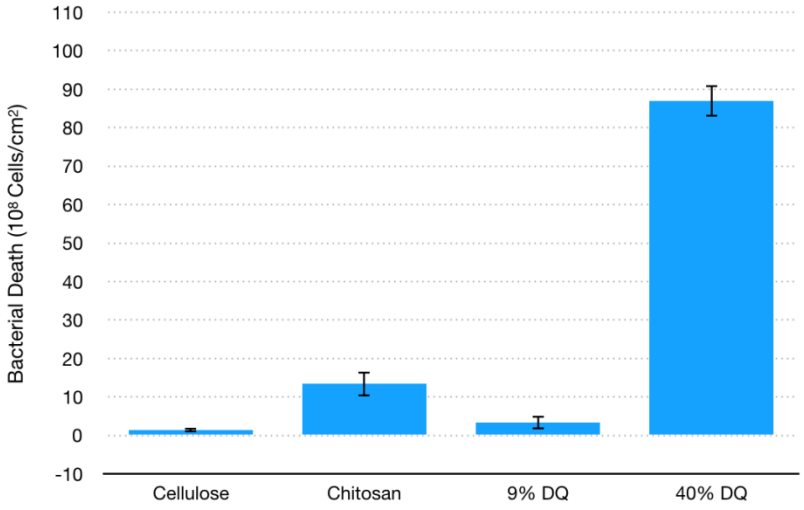

Figure 32 - Bacterial death among above hydrogel with and without casted chitosan.

Source: By the author.

4.8 Printing patterns

After the hydrogel's constitution in water, the line printed above the ionic liquid with the solution of chitosan derivative could not be visually differentiated from the other part constituted in water. So, we seeded the cells above the membranes and we were expecting a line separating two blank regions, where above the line we would observe the HFF-1 cells attached to it. However, it is only possible to observe fibroblast cells attach to control TCP plate (Figure 33 A-B) and none above the membrane (Figure 33 C-D). The cells did not attach to the surface membrane with highest DQ chitosan and apparently, they could have started programmed cell death, because there are tiny objects around 30 μm in diameter, which could be cell debris.

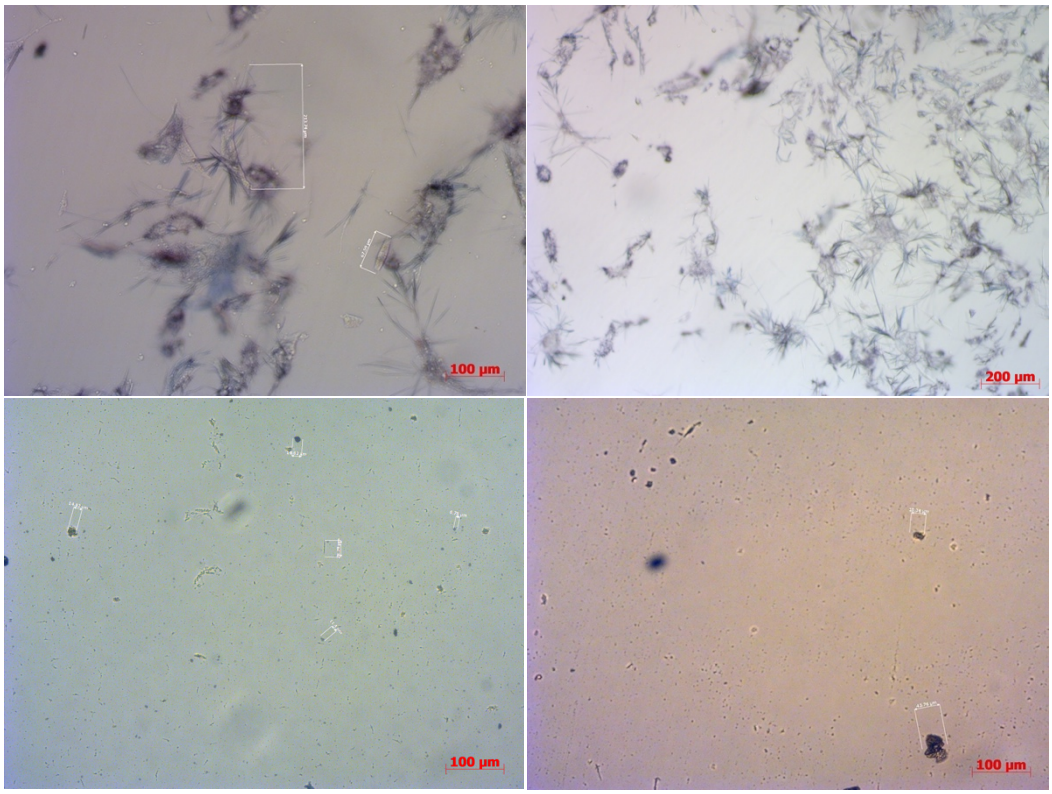

Figure 33 - A and B) Control shows formazan crystal inside HFF-1 cells and C and D) Membrane of 40% DQ of chitosan without any cell attach to it presenting some round shape objects.

Source: By the author.

4.9 Photobiomodulation test

In order to investigate the photobiomodulation effect against the HFF-1 cells, after each irradiation of 18J/cm^2, we imaged through optical microscope the cells behavior and MTT assay to assess the metabolic activity. This was the initial tests to verify the proliferation of cells when irradiating them with 660 nm.

The images after each irradiation (Figure 35 A, B, C) did not show any notable difference from number of cells and spreading compared with control group (Figure 35 D, E, F). This light fluence applied did not visually accelerated the cells replication. Although, there is a study revealing indirectly the cells proliferation for a lower light fluence of 3J/cm^2. (58) Also, the metabolic activity assay after the first 3 irradiations (Figure 34) presented a lower viability for cells compared with control group. This could be effect of cells exposed to PBS during the irradiation process.

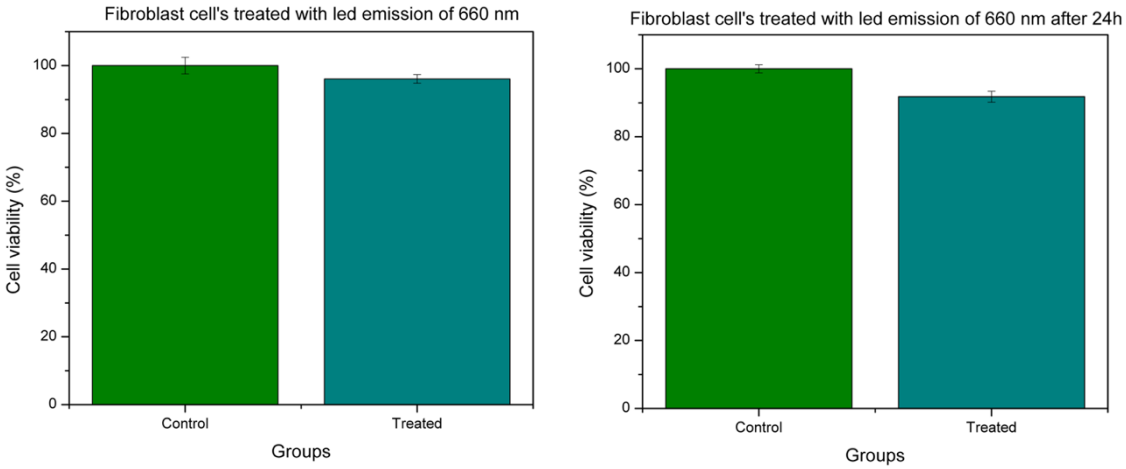

Figure 34 – MTT assay performed in HFF-1 cells a) after 3 light fluences of 18J/cm^2 and b) after 24h.

Source: By the author.

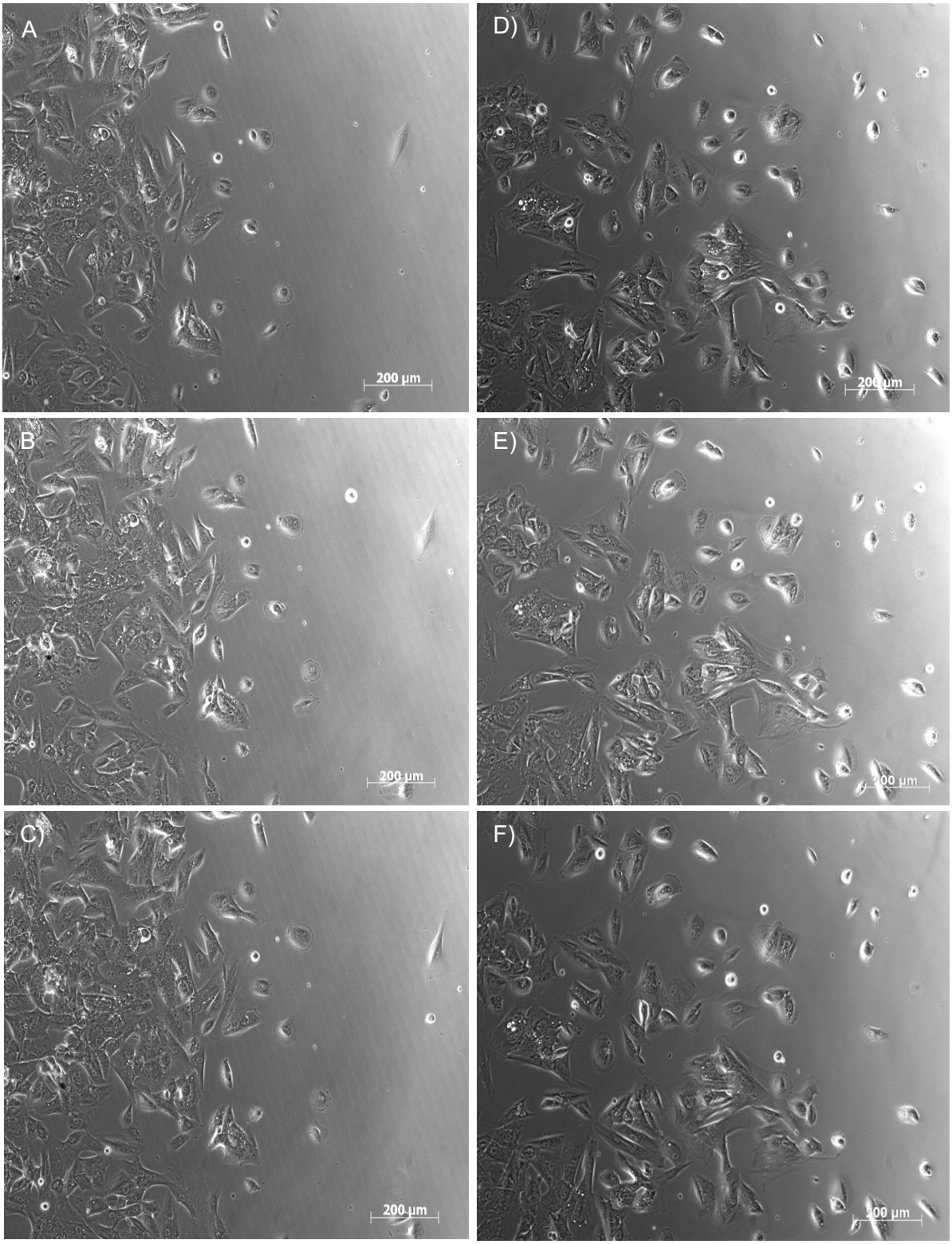

Figure 35 – Images of HFF-1 cells after irradiation with light fluence of 18J.cm^{-2} at 660 nm. After a) first, b) second and c) third irradiation. The respectively control without irradiation at same conditions after d) first, e) second and c) third irradiation.

Source: By the author.

5 CONCLUSION

The synthesis generated four different chloride chitosan derivatives observed at proton NRM, C13 and FT-IR spectrums. They revealed the reaction with ammonium group through the H-NMR shifts at H1 and transmittance at 1479 cm^{-1}. The degree of quaternization of chitosan, which represents the positive charges at the biopolymer chain, measured by H-NMR and titration technique presented similar results around with 10% and 40% DQ. All chitosan derivatives presented DD above 70%, which could increase the charges of the polymer depending the medium and potentially change the response of the biopolymer. The synthesis also produced biopolymer with molecular weight of 400kDa to 1000 kDa, which is not usually found.

Hydrogels generated from cellulose and chitosan derivatives proved to have a good interaction. From the beginning, the purple color of ninhydrin reaction evidenced the chitosan interaction with the cellulose polymer, interesting we were able to confirm this through confocal microscopy by seeing the chitosan fluorescence. Only the reaction with ninhydrin would not be possible to deduce the penetration inside the hydrogel, the confocal measurements was precise to reveal the chitosan derivatives was at the top and the bottom surface and at maximum 14 µm depth. The penetration depth was inversely proportional to the molecular size.

The positive charge from ammonium group inserted at chitosan affected the cells and bacteria behavior. We were able to see an increase of cell attachment proportionally to DQ. Hydrogels casted with chitosan derivative of 40% DQ presented, approximately, 60% of cell attachment compared to TCP plate and had the advantage to present similar results without growth factors and proteins to help to adhere. Also, the cells presented more spread shape with the increase of charges, indicating a good proliferation above those hydrogels. Although, the increase of positive charge above the material presented a higher antimicrobial activity, we also noticed the increase of attachment of E. coli to a hydrogel with higher DQ. This bacterium seems to use the dead ones as support to grow and proliferate. The molecular weight appeared to not influence the biological experiments.

Printing pattern above the material did not resulted in cell's attachment for the parameter we used, and more experiments are required. The use of this technique could help develop more complex materials. Photobiomodulation at 660 nm also did not presented proliferation results at this lights fluences, although there is potential to use synergistically with the material and cells.

Finally, this study demonstrated the good interaction between two low-cost biopolymers in generating a stable hydrogel. This material presented a good cell response without the use of growth factors and proteins at the manufacture. These results presented a good material to use in regenerative field.

REFERENCES

1 SHEVCHENKO, R. V.; JAMES, S. L.; JAMES, S. E. A review of tissue-engineered skin bioconstructs available for skin reconstruction. **Journal of The Royal Society Interface**, v. 7, n. 43, p. 229–258, 2010.

2 LEONG, K. G. *et al*. Generation of a prostate from a single adult stem cell. **Nature**, v. 456, n. 7223, p. 804–808, Dec. 2008.

3 SONG, J. J. *et al*. Regeneration and experimental orthotopic transplantation of a bioengineered kidney. **Nature medicine**, v. 19, n. 5, p. 646–51, May 2013.

4 OTT, H. C. *et al*. Regeneration and orthotopic transplantation of a bioartificial lung. **Nature Medicine**, v. 16, n. 8, p. 927–933, Aug. 2010.

5 OTT, H. C. *et al*. Perfusion-decellularized matrix: using nature's platform to engineer a bioartificial heart. **Nature Medicine**, v. 14, n. 2, p. 213–221, Feb. 2008.

6 BAJAJ, P. *et al*. 3D biofabrication strategies for tissue engineering and regenerative medicine. **Annual Review of Biomedical Engineering**, v. 16, p. 247–76, July 2014.

7 BONES made with 3D printer. **Nature**, v. 538, n. 7623, p. 8–8, Oct. 2016. DOI: 10.1038/538008a.

8 MIRZAEI, M. *et al*. Protein-based 3D biofabrication of biomaterials. **Bioengineering**, v. 8, n. 4, p. 48, Apr. 2021.

9 FONG, P. M.; PARK, J.; KANE BREUER, C. Heart valves. *In*: LANZA, R.; LANGER, R.; VACANTI, J. (ed.). **Principles of tissue engineering**. Amsterdam: Elsevier, 2007. p. 585–601.

10 COURTENAY, J. C. *et al*. Surface modified cellulose scaffolds for tissue engineering. **Cellulose**, v. 24, n. 1, p. 253–267, Jan. 2017.

11 JOHNS, M. A. *et al*. Predicting ligand-free cell attachment on next-generation cellulose–chitosan hydrogels. **ACS Omega**, v. 3, n. 1, p. 937–945, Jan. 2018.

12 NEUROTIKER. **Cellulose structure**. Available from: https://pt.wikipedia.org/wiki/Celulose#/media/Ficheiro:Cellulose_Sessel.svg. Accessible at: Jan.1, 2022.

13 NEUROTIKER. **Chitin reaction**. Available from: https://en.wikipedia.org/wiki/File:Chitosan_Synthese.svg. Accessible at: Jan.1 2022.

14 ARIAS, C. J.; SURMAITIS, R. L.; SCHLENOFF, J. B. Cell adhesion and proliferation on the "living" surface of a polyelectrolyte multilayer. **Langmuir**, v. 32, n. 21, p. 5412, 2016.

15 CHEN, L. *et al*. The role of surface charge on the uptake and biocompatibility of hydroxyapatite nanoparticles with osteoblast cells. **Nanotechnology**, v. 22, n. 10, p. 105708, Mar. 2011.

16 LALLI, M. L.; ASTHAGIRI, A. R. Collective migration exhibits greater sensitivity but slower dynamics of alignment to applied electric fields. **Cell and Molecular Bioengineering**, v. 8, n.2, p. 247-257, 2015.

17 SAJOMSANG, W. *et al*. Quaternization of N-aryl chitosan derivatives: synthesis, characterization, and antibacterial activity. **Carbohydrate Research**, v. 344, n. 18, p. 2502–2511, Dec. 2009.

18 DASH, M. *et al*. Chitosanâ€"A versatile semi-synthetic polymer in biomedical applications. **Progress in Polymer Science**, v. 36, p. 981–1014, 2011. DOI:10.1016/J.PROGPOLYMSCI.2011.02.001.

19 ATAY, H. Y. Antibacterial activity of chitosan-based systems. *In*: JANA, S.; JANA, S. (ed.). **Functional chitosan**. Singapore: Springer, 2019. p. 457–489.

20 FIAMINGO, A. *et al*. Extensively deacetylated high molecular weight chitosan from the multistep ultrasound-assisted deacetylation of beta-chitin. **Ultrasonics Sonochemistry**, v. 32, p. 79–85, 2016. DOI: 10.1016/j.ultsonch.2016.02.021.

21 ISHIZAKI, T.; SAITO, N.; TAKAI, O. Correlation of cell adhesive behaviors on superhydrophobic, superhydrophilic, and micropatterned superhydrophobic/superhydrophilic surfaces to their surface chemistry. **Langmuir**, v. 26, n. 11, p. 8147–8154, June 2010.

22 DOWLING, D. P. *et al*. Effect of surface wettability and topography on the adhesion of osteosarcoma cells on plasma-modified polystyrene. **Journal of Biomaterials Applications**, v. 26, n. 3, p. 327–347, Sept. 2011.

23 JOHNS, M. A. *et al*. Predicting ligand-free cell attachment on next-generation cellulose-chitosan hydrogels. **ACS omega**, v. 3, n. 1, p. 937–945, Jan. 2018.

24 LIN, W. C. *et al.* Bacterial cellulose and bacterial cellulose-chitosan membranes for wound dressing applications. **Carbohydrate Polymers**, v. 94, n. 1, p. 603–611, 2013.

25 DEMITRI, C. *et al*. Cellulose-based porous scaffold for bone tissue engineering applications: Assessment of hMSC proliferation and differentiation. **Journal of Biomedical Materials Research Part A**, v. 104, n. 3, p. 726–733, Mar. 2016.

26 ZHAO, D. *et al.* Biomedical applications of chitosan and its derivative nanoparticles. **Polymers**, v. 10, n. 4, Apr. 2018.

27 PÉRTILE, R. *et al*. Bacterial cellulose modified using recombinant proteins to improve neuronal and mesenchymal cell adhesion. **Biotechnology Progress**, v. 28, n. 2, p. 526–532, Mar. 2012.

28 PERTILE, R. A. N. *et al*. Surface modification of bacterial cellulose by nitrogen-containing plasma for improved interaction with cells. **Carbohydrate Polymers**, v. 82, n. 3, p. 692–698, Oct. 2010.

29 ANDRADE, F. K. *et al*. Improving the affinity of fibroblasts for bacterial cellulose using carbohydrate-binding modules fused to RGD. **Journal of Biomedical Materials Research Part A**, v. 92A, n. 1, p. 9–17, Jan. 2010.

30 CROISIER, F.; JÉRÔME, C. Chitosan-based biomaterials for tissue engineering. **European Polymer Journal**, v. 49, n. 4, p. 780–792, Apr. 2013.

31 DYAWANAPELLY, S. *et al.* Improved mucoadhesion and cell uptake of chitosan and chitosan oligosaccharide surface-modified polymer nanoparticles for mucosal delivery of proteins. **Drug Delivery and Translational Research**, v. 6, n. 4, p. 365–79, Apr. 2016.

32 LIU, X. *et al*. Multidentate zwitterionic chitosan oligosaccharide modified gold nanoparticles: stability, biocompatibility and cell interactions. **Nanoscale**, v. 5, n. 9, p. 3982, May 2013.

33 WEBB, A. R.; YANG, J.; AMEER, G. A. Biodegradable polyester elastomers in tissue engineering. **Expert Opinion on Biological Therapy**, v. 4, n. 6, p. 801–812, June 2004.

34 BREULS, R. G. M.; JIYA, T. U.; SMIT, T. H. Scaffold stiffness influences cell behavior: opportunities for skeletal tissue engineering. **Open Orthopaedics Journal**, v. 2, p. 103–109, May 2008.

35 MCKEE, C. T. *et al*. Indentation versus tensile measurements of Young's modulus for soft biological tissues. **Tissue Engineering Part B:** reviews, v. 17, n. 3, p. 155–164, June 2011.

36 SHEN, X. *et al*. Hydrogels based on cellulose and chitin: fabrication, properties, and applications. **Green Chemistry**, v. 18, n. 1, p. 53–75, Dec. 2016.

37 SHARMA, R. I.; SHREIBER, D. I.; MOGHE, P. V. Nanoscale variation of bioadhesive substrates as a tool for engineering of cell matrix assembly. **Tissue Engineering Part A**, v. 14, n. 7, p. 1237–1250, July 2008.

38 SHIN, E. J. *et al*. Functionalizing cellulose scaffold prepared by ionic liquid with bovine serum albumin for biomedical application. **Fibers and Polymers**, v. 14, n. 12, p. 1965–1969, 2013.

39 SANTOS, D. M.; BUKZEM, A. L.; CAMPANA-FILHO, S. P. Response surface methodology applied to the study of the microwave-assisted synthesis of quaternized chitosan. **Carbohydrate Polymers**, v. 138, p. 317–326, Mar. 2016.

40 FERREIRA, E. S. *et al*. Adhesive and reinforcing properties of soluble cellulose: a repulpable adhesive for wet and dry cellulosic substrates. **ACS Applied Materials & Interfaces**, v. 7, n. 33, p. 18750–18758, Aug. 2015.

41 GOUVEIA, R. F.; GALEMBECK, F. Electrostatic charging of hydrophilic particles due to water adsorption. **Journal of the American Chemical Society**, v. 131, n. 32, p. 11381–11386, Aug. 2009.

42 NEČAS, D.; KLAPETEK, P. Gwyddion: an open-source software for SPM data analysis. **Open Physics**, v. 10, n. 1, p. 181–188, Jan. 2012.

43 RUEDEN, C. T. *et al*. ImageJ2: imageJ for the next generation of scientific image data. **BMC Bioinformatics**, v. 18, n. 1, p. 529, Dec. 2017.

44 LAVERTU, M. *et al*. A validated 1H NMR method for the determination of the degree of deacetylation of chitosan. **Journal of Pharmaceutical and Biomedical Analysis**, v. 32, n. 6, p. 1149–58, Aug. 2003.

45 ROBERTS, G. A. F. **Chitin chemistry**. London : Macmillan, 1992.

46 HUA, C. *et al*. The effect of low and high molecular weight chitosan on the control of gray mold (Botrytis cinerea) on kiwifruit and host response. **Scientia Horticulturae**, v. 246, p. 700–709, Feb. 2019.

47 COQUERY, C. *et al*. Synthesis of new high molecular weight phosphorylated chitosans for improving corrosion protection. **Pure and Applied Chemistry**, v. 91, n. 3, p. 509–521, Mar. 2019.

48 CHEAH, W. Y. *et al.* Antibacterial activity of quaternized chitosan modified nanofiber membrane. **International Journal of Biological Macromolecules**, v. 126, p. 569–577, Apr. 2019.

49 DOMARD, A. *et al*. 13C and 1H n.m.r. spectroscopy of chitosan and N-trimethyl chloride derivatives. **International Journal of Biological Macromolecules**, v. 9, n. 4, p. 233–237, 1987.

50 EISENBERG, S. *et al*. Mapping the electrostatic profiles of cellular membranes. **Molecular Biology of the Cell**, v. 32, n. 3, p. 301–310, Feb. 2021.

51 ZAREIDOOST, A. *et al*. The relationship of surface roughness and cell response of chemical surface modification of titanium. **Journal of Materials Science**: materials in medicine, v. 23, n. 6, p. 1479–88, June 2012.

52 BIAZAR, E. *et al*. The relationship between cellular adhesion and surface roughness in polystyrene modified by microwave plasma radiation. **International Journal of Nanomedicine**, v. 6, p. 631–9, 2011. DOI: 10.2147/IJN.S17218.

53 LI, G.-F. *et al*. Preparation and testing of quaternized chitosan nanoparticles as gene delivery vehicles. **Applied Biochemistry and Biotechnology**, v. 175, n. 7, p. 3244–3257, Apr. 2015.

54 JAEPYOUNG, C. *et al*. Synthesis and physicochemical and dynamic mechanical properties of a water-soluble chitosan derivative as a biomaterial. **Biomacromolecules**, v. 7, n. 10, p. 2845, 2006.

55 KIM, S.-K. **Chitin, chitosan, oligosaccharides and their derivatives :** biological activities and applications. Boca Raton: CRC Press, 2011.

56 ELUL, R. Fixed charge in the cell membrane. **Journal of Physiology**, v. 189, n. 3, p. 351–65, Apr. 1967.

57 REBL, H. *et al.* Positively charged material surfaces generated by plasma polymerized allylamine enhance vinculin mobility in vital human osteoblastss. **Advanced Engineering Materials**, v. 12, n. 8, p. B356–B364, Aug. 2010.

58 WANG, Y. *et al*. Red (660 nm) or near-infrared (810 nm) photobiomodulation stimulates, while blue (415 nm), green (540 nm) light inhibits proliferation in human adipose-derived stem cells. **Scientific Reports**, v. 7, n. 1, p. 7781, 2017.

APPENDIX A – IMAGES OF CELL MORPHOLOGY

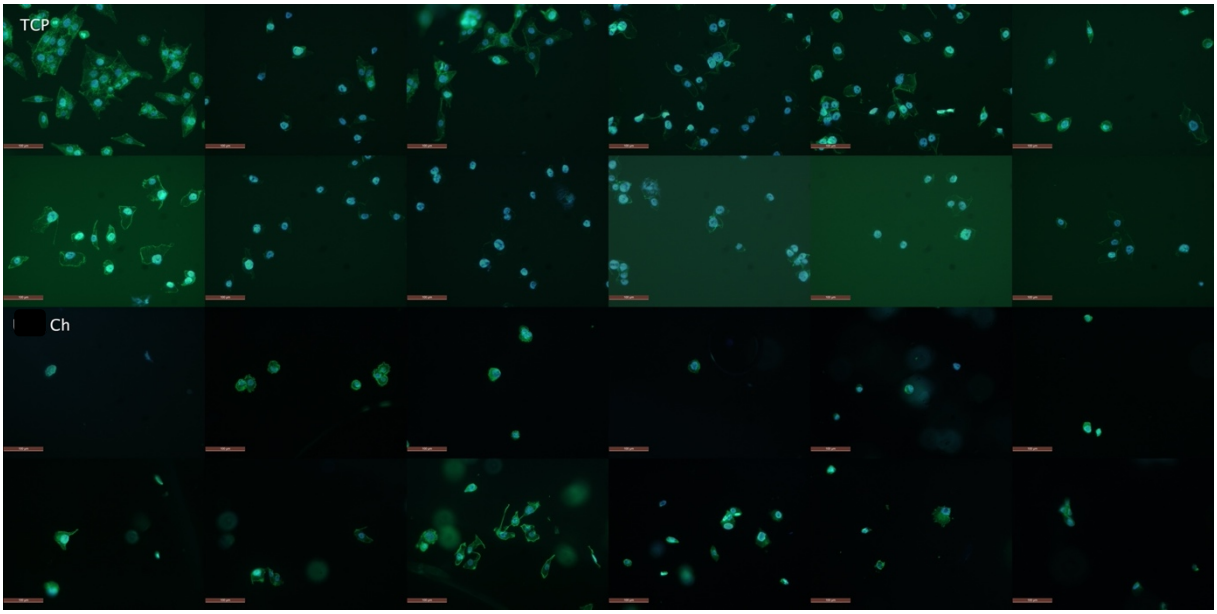

Figure 36 – Fluorescence images of cell's morphology of MG-63 stained with phalloidins (green) and DAPI (blue) for TCP plate and hydrogel casted with chitosan. The first 12 images are from TCP and the next 12 images belongs to hydrogel casted with chitosan.

Source: By the author.

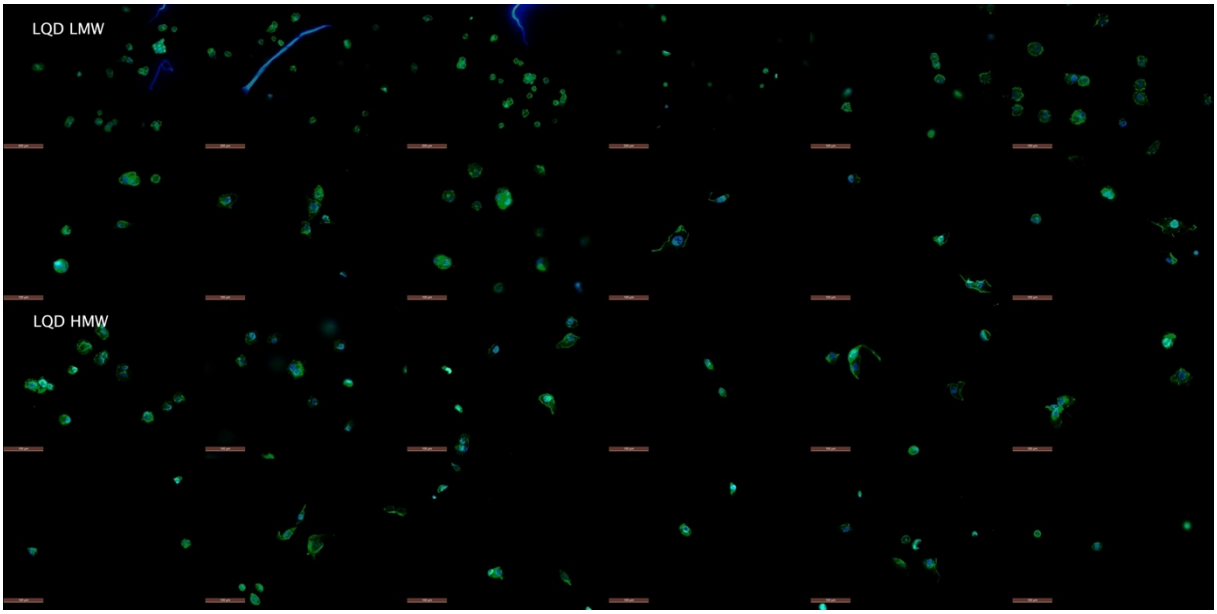

Figure 37 – Fluorescence images of cell's morphology of MG-63 stained with phalloidins (green) and DAPI (blue). The first 12 images are from hydrogels casted with QCh of low (10%) DQ and low () MW and the next 12 images belongs to hydrogel casted with QCh of low (10%) DQ and high () MW.

Source: By the author.

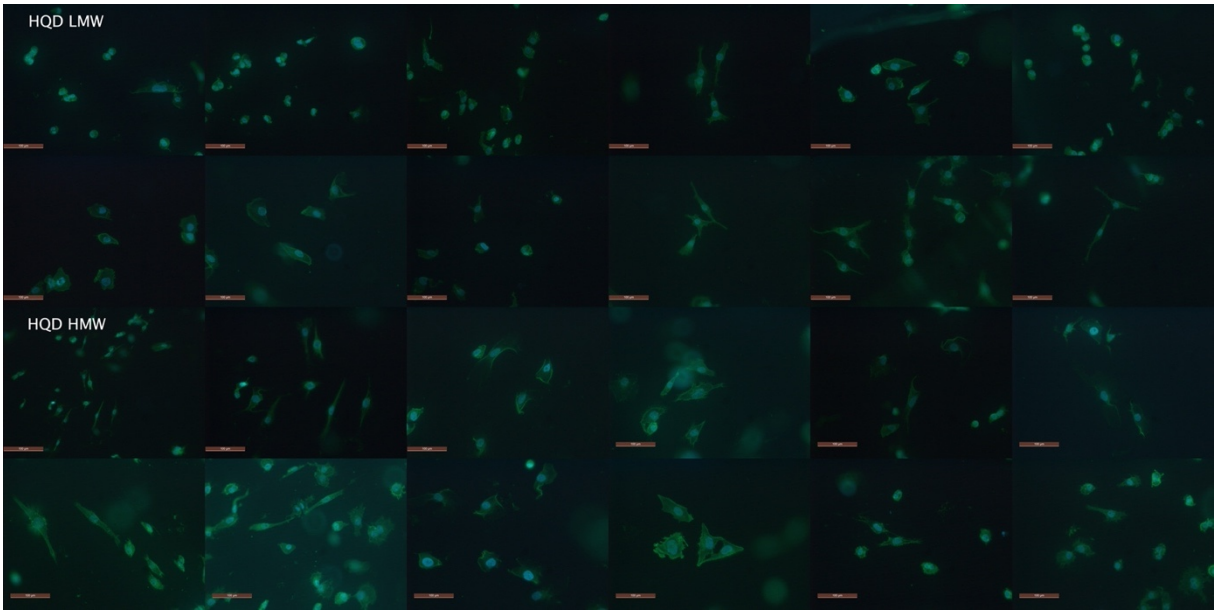

Figure 38 – Fluorescence images of cell's morphology of MG-63 stained with phalloidins (green) and DAPI (blue). The first 12 images are from hydrogels casted with QCh of high (40%) DQ and low () MW and the next 12 images belongs to hydrogel casted with QCh of high (40%) DQ and high () MW.

Source: By the author.